Journal of
Cerebral Blood Flow
& Metabolism

Arterial Spin Labeling for Measurement of Cerebral Perfusion and Angiography

Journal:	*Journal of Cerebral Blood Flow and Metabolism*
Manuscript ID	JCBFM-0357-17-REV.R1
Manuscript Type:	Review Article
Date Submitted by the Author:	n/a
Complete List of Authors:	Jezzard, Peter; University of Oxford, Wellcome Trust Centre for Integrative Neuroimaging Chappell, Michael; University of Oxford, Institute of Biomedical Engineering Okell, Thomas; FMRIB Centre, Nuffield Department of Clinical Neurosciences, University of Oxford
Research Topics:	MRI, Cerebral Blood Flow, Atherosclerosis, Acute Stroke, Brain Imaging, Stroke, Arteriovenous Malformations
Research Techniques:	Arterial spin labelling, ASL, MRI, MR Angiography, CBF measurement, Imaging, Magnetic Resonance Imaging/Spectrocopy

Arterial Spin Labeling for Measurement of Cerebral Perfusion and Angiography

Peter Jezzard,[1,*] Michael A. Chappell[2] and Thomas W. Okell[1]

[1]Wellcome Centre for Integrative Neuroimaging, FMRIB Division, Nuffield Dept of Clinical Neurosciences, University of Oxford, UK
[2]Institute of Biomedical Engineering, University of Oxford, UK

Word Count: 7985 words

[*]Address for Correspondence:

Peter Jezzard, PhD
Wellcome Centre for Integrative Neuroimaging
FMRIB Division, NDCN, University of Oxford
John Radcliffe Hospital
Oxford
OX3 9DU
United Kingdom

Phone: +44 [0]1865 222727
Fax: +44 [0]1865 222717
Email: peter.jezzard@univ.ox.ac.uk

Funding sources: Dunhill Medical Trust (grant OSRP1/1006), Engineering and Physical Sciences Research Council (grant EP/P012361/1), Royal Academy of Engineering and Wellcome Trust (grant 203139/Z/16/Z).

Running Header: Review of arterial spin labeling MRI methods

Abstract

Arterial spin labeling (ASL) is an MRI technique that was first proposed a quarter of a century ago. It offers the prospect of non-invasive quantitative measurement of cerebral perfusion, making it potentially very useful for research and clinical studies, particularly where multiple longitudinal measurements are required. However, it has suffered from a number of challenges, including a relatively low signal-to-noise ratio, and a confusing number of sequence variants, thus hindering its clinical uptake. Recently, however, there has been a consensus adoption of an accepted acquisition and analysis framework for ASL, and thus a better penetration onto clinical MRI scanners. Here, we review the basic concepts in ASL, and describe the current state-of-the-art acquisition and analysis approaches, and the versatility of the method to perform both quantitative cerebral perfusion measurement, along with quantitative cerebral angiographic measurement.

Key Words: MRI, perfusion imaging, arterial spin labeling, angiography

Introduction and Historical Perspective

Magnetic resonance imaging (MRI) has a long history of measuring blood flow in large vessels. This includes the development of time-of-flight angiography[1] to visualize the brain's vasculature, as well as more quantitative measurements of luminal blood velocity via phase contrast methods.[2] However, none of these methods measures delivery of blood to the tissue itself, and therefore the health of the brain at the level of the capillary bed. Methods such as xenon computed tomography[3] (CT), ^{15}O positron emission tomography[4,5] (PET), and CT perfusion were available at this time but these methods all involved exposure to ionizing radiation. An early MRI method to attempt capillary-level perfusion measurement was intravoxel incoherent motion (IVIM) developed by LeBihan and colleagues.[6] For this, blood flow at the microscopic level was modeled as a pseudo-diffusion process, with the blood displacements in the capillary bed having a relatively large apparent diffusion coefficient relative to water in tissue. It was hypothesized that perfusion could be extracted from a two-compartment fit of signal versus increasing diffusion encoding (b-value), with the blood compartment showing strong signal attenuation at low b-values. However, in practice the low blood volume fraction in brain tissue, along with difficulties obtaining clean model separation between blood and tissue compartments, meant that IVIM never succeeded in its goal of measuring cerebral perfusion (although it has found success in other organ systems and in certain pathologies).

Another MRI approach to measuring cerebral perfusion is dynamic susceptibility contrast (DSC). This is more invasive, requiring injection of a bolus of gadolinium chelate contrast agent and subsequently imaging the bolus passage through the tissue bed.[7,8] Gadolinium contrast agents lead to microscopic magnetic field inhomogeneities in the surrounding tissue as they pass through the capillary bed, and hence to a faster signal decay. Although theoretically possible to measure tissue perfusion, DSC suffers from a variety of practical limitations, not least the need to accurately de-convolve a local arterial input function[9]. As such, it has found application in the measurement of relative cerebral blood volume, and in assessing ischaemia via arrival time delays, but although able to measure relative cerebral perfusion it has struggled to offer a truly absolute measurement of perfusion.[10] A final method worth mentioning is that of perfusion mapping using 17-oxygen water, which can yield quantitative perfusion measurements,[11] but is hard to scale up to human use due to the expense of the labeled agent.

The approach of arterial spin labeling (ASL) for imaging cerebral perfusion was first demonstrated in the early 1990s,[12] although the overall principles can be traced back to 1959.[13] Inspired by spectroscopic tracer kinetic methods,[14-16] (and utilizing flow-driven adiabatic fast passage to invert the blood spins, contrasted with an image in which the blood spins are left un-inverted – already successfully used for angiographic purposes previously by Dixon and colleagues[17]), the detection of magnetically labeled blood in rat brain was used to extract quantitative measures of perfusion.[18] Initially, blood saturation was used, rather than inversion (yielding lower signal-to-noise ratio),[19] but later a flow-driven adiabatic inversion principle was used in human brain,[20] and the field of ASL MRI was born.

Subsequent papers demonstrated other variations of the underlying principles. As well as flow-driven adiabatic inversion, that establishes a 'continuous ASL' steady-state

delivery of inverted blood water spins to the tissue, it was shown that a slab of inverted spins could also be used to provide ASL contrast. One such 'pulsed ASL' method is the EPI signal targeting with alternating RF (EPISTAR) method,[21] yielding qualitative perfusion by taking the signal difference between an image acquired following a proximal slab inversion of blood spins, versus one acquired with no inversion pulse. A later variant of this method was the PICORE method of Wong et al.[22] This used an off-resonance control pulse, rather than no control RF pulse (as in the original EPISTAR method) or a distal slab inversion (as in subsequent EPISTAR implementations). The advantage is that only proximal arterial blood is labeled, rather than both proximal arterial and distal venous blood. Another form of pulsed ASL is the flow-sensitive alternative inversion (FAIR) method.[23-25] This takes difference images acquired after a slice-selective versus non-slice-selective inversion, again enabling difference images that reflect perfusion.

A difficulty with these early methods is that they do not lend themselves to multi-slice acquisition. In the case of continuous ASL methods, a control RF pulse is needed with matched magnetization transfer[26] effects, and the frequency condition for this matching could only be achieved for a single slice location. Likewise, pulsed ASL methods suffered either from unwanted direct perturbation of the imaging slices by the labeling pulse, or due to a limited amount of blood labeled in the region proximal to the imaging slices. A significant step forward was made by Alsop and Detre[27] with a continuous ASL scheme that matched MT effects across multiple slices. More recently, the invention of pseudo-continuous labeling,[28] involving a train of multiple low angle selective RF pulses, has allowed the higher signal-to-noise (SNR) of continuous ASL to be implemented on a modern clinical scanner (on which a 'true' continuous RF pulse is challenging in practice).

Physical Principles of ASL

The principal sub-categories of ASL are pulsed ASL (PASL) and continuous ASL (CASL). More recently, further forms of ASL have been described, such as velocity-selective ASL (vsASL) and pseudo-continuous ASL (pCASL). Indeed, the latter method offers many attractive features and has become the accepted 'standard' acquisition strategy. As such, the pCASL method will be summarized first, with a briefer mention made of the original CASL method and the PASL method.

Pseudo-continuous arterial spin labeling (pCASL)

The main clinically relevant method the ASL armoury for clinical deployment is pseudo-continuous ASL (pCASL).[28] This offers relatively good SNR and can be deployed using standard clinical MRI hardware. This has made it the labeling method advocated by the ISMRM Perfusion Study Group and the European Consortium for ASL in Dementia.[29] The basic principle is shown in Fig. 1a. Adiabatic inversion of the blood magnetization as it passes through the labeling plane is achieved via a mechanism different from the original CASL method. Figure 1a shows a train of closely spaced low flip-angle slice-selective RF pulses, in conjunction with suitable gradients orientated in the direction of flow. The time-averaged values for the RF pulses and gradient pulses for pCASL are similar to the values needed for standard CASL. However, in the case of pCASL the transition of the spins from alignment along $+z$ to $-z$ is most easily thought of in terms of

the off-resonance magnetization profile familiar from steady-state free precession pulse sequences.[30]

For a steady-state train of RF pulses, with a phase evolution of ϕ between consecutive pulses, the steady-state longitudinal (M_z) profile (neglecting T1 and T2 effects) is given by:[31]

$$M_z = \frac{\pm M_0 \sin\alpha \sin(\phi/2)}{\sqrt{(1-\cos\alpha)^2 + \sin^2\alpha \sin^2(\phi/2)}}$$

This function is shown in Fig. 1b for an RF flip angle, α, of 20°, displaying a repeating pattern of modulations in M_z as a function of ϕ (which can also be thought of as phase accumulated due to the spin being off-resonance). Considering now a moving spin that is initially off-resonance with respect to the RF pulses (i.e., at the far left of Fig. 1b), its M_z will be modulated by the steady-state pulse train. Under appropriate conditions of flow velocity to achieve adiabatic conditions, and RF pulse bandwidth such that only the central M_z transition (shown in red) in Fig. 1b exerts influence on the moving spins, the magnetization will invert as it passes through the labeling plane. For the control condition the phase of consecutive RF pulses needs only to be advanced by 180° (shown in Fig. 1a). This ensures that the steady-state is not established, since the net flip angle in the pulse train becomes zero.

[INSERT FIGURE 1 ABOUT HERE]

One source of error for pCASL is caused by poor shim, when the assumed phase evolution between the labeling RF pulses, ϕ, may not hold true. This results in a shift of the effective labeling plane location, and for a large enough shift this will reduce the RF field experienced at the new labeling plane location to such an extent that adiabatic inversion is compromised, or possibly extinguished. Strategies to mitigate this are either: (i) to ensure that the labeling region is well shimmed or in a region of inherently good shim (e.g., the region of the neck where the two internal carotid and two vertebral arteries run approximately perpendicular to the transverse plane); or (ii) to run the experiment multiple times, with progressively greater phase shift added between the RF pulses,[32] for example by running n repeats, with $\Delta\phi = 2\pi/n$; or (iii) by incorporating transverse gradient blips into the pCASL train to spatially compensate for erroneous phase shifts[33] (the same principle used for vessel-encoded pCASL, as described later).

Continuous arterial spin labeling (CASL)

The original CASL method also relied on flow-driven adiabatic inversion of moving blood, but using a true (or near-true) continuous RF pulse. Figure 2a shows the typical labeling strategy used for CASL acquisition. The inversion time (TI, also known as the post-label delay or PLD) allows time for labeled blood water to arrive at the slice of interest. As blood water spins approach the labeling plane they initially are too off-resonance to be affected by the RF pulse, and so experience an effective field that is simply a property of being off-resonance (directed predominantly along z). When closer to the labeling plane the off-resonance approaches zero, and the spins experience a progressively 'on-resonance' radiofrequency field (now predominantly in the x-y plane).

Then, as they pass though the labeling plane and move towards the imaging slice the effective field once more becomes off-resonance and is directed along -*z*. Under appropriate 'adiabatic' conditions, the blood water magnetization vector is 'locked' to the effective field, and is tipped from (equilibrium) M_z=M_0 into an inverted M_z=-M_0 state as it pass through the labeling plane.

A suitable combination of field gradient and RF field strength can be found that satisfies the required adiabatic conditions, given typical carotid artery blood velocities and NMR relaxation times. Indeed, theoretical and experimental measurements[34] of the labeling efficiency have yielded values of over 90%.

A number of practical obstacles prevent the original CASL method being clinically useful, however. One is that the RF amplifiers of most clinical MRI scanners cannot deliver a continuous RF pulse (even at low power). Another issue is that the conventional CASL method is inherently single-slice, since it is strongly affected by magnetization transfer (MT) effects. To counter this, a control acquisition is needed with an RF pulse played out equidistant but distal to the imaging plane. However, only one slice location satisfies this condition. A solution is to use a separate small labeling coil positioned against the neck,[35,36] so that MT effects are not experienced by the imaging slices, although this is cumbersome to implement on a clinical scanner. Another solution is to modify the control pulse by cosine-modulating the 'continuous' RF signal, such that a 'double' inversion profile is achieved,[27] whilst ensuring that MT effects are matched to the labeling pulse. The second inversion plane has the effect of un-inverting the spins from the first inversion plane, although labeling efficiency and SNR is lost.

[INSERT FIGURE 2 ABOUT HERE]

Pulsed arterial spin labeling (PASL)

The principles of PASL are shown in Figs 2b and 2c, showing two variants of PASL (PICORE[22] and FAIR[24]), respectively. PICORE has the advantage of labeling only proximal arterial spins, whereas FAIR labels both proximal and distal spins. Both have potential difficulties with the slab profile being non-ideal, leading to slice-to-slice systematic artifacts.

A further extension to the PICORE method is the QUIPSS II sequence of Wong et al.[37] in which an additional saturation pulse is added a time TI1 after the inversion pulse (see Fig. 2d). Having the same spatial profile as the inversion, and played out for both the labeling images and the control images, its purpose is to curtail the labeled bolus and provide a well-characterized temporal duration, given by the time TI1. Indeed, provided the time TI2-TI1 (see Fig. 2d) is sufficiently long that all labeled blood has been delivered to the tissue (i.e. TI2-TI1>δt, where δt is the arterial transit time), a quantitative image of perfusion can be obtained using a single QUIPSS II acquisition.

Additional pulse sequence considerations

A variety of image readout strategies have been used, with a preference for 'snap-shot' methods that acquire the data rapidly, and allow some signal-averaging to be adopted. Echo planar imaging[38] (EPI) has been widely used, with its well-known advantages

(speed, SNR) and disadvantages (geometric distortion). One issue that must be borne in mind with multi-slice approaches is that the effective post-labeling delay varies for different slice positions, and this must be accounted for in the analysis. Snap-shot 3D acquisitions[39,40,41] overcome this issue, although slice coverage and image resolution are limited using such methods. Segmenting the readout across different acquisition can help to provide more coverage, although is more prone to artifacts from subject motion, but is the optimal solution advocated in the ISMRM/EU consensus paper.[29]

ASL is an inherently low SNR method, since the accumulation of labeled magnetization due to the delivery of tagged blood is small compared to the static tissue magnetization. One particularly helpful strategy to improve sensitivity is to use background suppression of static spins. In theory the signal from static tissue should subtract when taking the difference between the control and the labeled images. However, any mis-registration or physiological noise present in the raw data can risk swamping the ASL signal. For this reason it is desirable to null the static signal, without affecting the blood signal. This can be accomplished using additional, strategically placed, global inversion pulses,[42-44] known as the ASSIST method. ASSIST saturates the magnetization in the imaging plane at the time of the initial label inversion, and then includes subsequent non-selective inversion pulses during the inversion delay period that are timed to ensure the static tissue is passing close to its signal null point at the time of image acquisition. An additional advantage of including the initial spatial saturation of the imaging slices is that any direct excitation effects of the labeling inversion pulse on the imaging slices is minimized. The ASSIST method is particularly useful for 3D acquisitions, where a single readout excitation pulse is used, but is also useful in 2D multi-slice acquisitions and for segmented acquisitions.

A problem common to all ASL methods is their sensitivity to motion due to the subtraction of label and control images. Motion-induced static tissue signal changes cause imperfect subtraction and result in artefact appearing in the perfusion maps. *Post-hoc* motion correction can be helpful, although intra-volume motion will still result in residual artifacts. Efficient background suppression, such as ASSIST, reduces static tissue signal and therefore motion artifacts, although some residual tissue signal is useful for *post-hoc* motion correction. Prospective motion correction techniques using navigators to estimate and correct for subject motion show some promise.[45,46] In addition, there are a number of approaches for identifying problematic raw data, allowing its filtering or rejection.[47-50]

Advanced Labeling Schemes

Following description of the main variants on the ASL theme, some additional 'flavours' deserve mention, with further advances described recently in a related review.[51]

Multi-delay and time-encoded preparations

Conventional ASL protocols acquire multiple label and control images at a fixed delay after labeling, which are then averaged in post-processing. In order for the subtraction images to have signal intensity proportional to tissue perfusion, all labeled blood must reach the tissue prior to image acquisition.[52] However, the arterial transit time (ATT) for blood arrival is not known *a-priori* and may be prolonged in patients with vascular disease. Use of a very long delay mitigates this problem to some degree,[53] but also

degrades image quality due to the increased T1 decay of the labeled blood, and hence poorer SNR.

An alternative approach is to acquire images at a range of different delays, allowing visualization of the dynamics of blood flow into the tissue. A kinetic model can be fitted to the data to estimate ATT and perfusion (see below) without the assumption that all labeled blood has reached the tissue at a particular delay time. Although the number of signal averages at any particular delay time is reduced in this approach, all of the information across delays can be pooled during the model fitting process to enable accurate perfusion estimates to be derived. Also, the necessity to sample only at long delay can be dropped, allowing the signal to be sampled closer to its peak intensity, which can increase SNR efficiency. However, the post-processing required for multi-delay approaches is considerably more complex than single-delay methods. At present the approach recommended in the ISMRM/EU consensus paper[29] is to use a fixed delay of 2000ms, unless there is reason to measure the arterial transit time.

If ATT is desired there are various strategies for multi-delay ASL, as shown in Figure 3. The simplest involves the separate acquisition of label and control images at different delay times.[52] An alternative approach[54] utilizes a readout scheme in which labeled blood is imaged at multiple time points following a single label pulse,[55,56] generating images at different effective delays. However, the reduced readout flip angle also reduces the SNR and the number of slices achievable is limited by the desired temporal resolution, restricting spatial coverage.

Another promising technique is time-encoded ('Hadamard-encoded') ASL.[57–60] Here the ASL labeling period is split into a series of blocks prior to image acquisition. These blocks are alternated between label and control states in different combinations across a series of imaging cycles according to a Hadamard encoding matrix. The perfusion signal arising from each individual block can be calculated in post-processing using a matrix inversion, yielding a series of images at different effective delay times. In this way N perfusion images can be derived from N+1 measurements, rather than the 2N required by standard multi-delay protocols. Additionally, the combination of signals across all imaging cycles results in improved noise averaging, although the perfusion signal arising from each block is generally reduced due to the shortened effective labeling duration. This can be partially compensated for by using variable block durations which trade off temporal resolution for improved signal strength.[60]

[INSERT FIGURE 3 ABOUT HERE]

Velocity-selective arterial spin labeling (vsASL)

A potential problem with the 'standard' forms of ASL described above is that if blood flow is severely delayed, or if there is significant collateral flow, the label may have decayed by T1 processes before it arrives at the imaging plane, and hence a perfusion absence may be concluded despite there actually being perfusion present. An intriguing alternative form of label preparation that may help address this deficiency, albeit a method that is still under development, is the concept of velocity-selective ASL.[61] The idea is to label spins on the basis of their velocity profile, rather than their spatial position. In the original vsASL sequence spins above a critical velocity, v_c, are labeled. Then, during the subsequent readout spins above v_c are crushed. The goal is to target

spins that decelerate from above v_c to below v_c in a velocity regime that corresponds to small arteries and arterioles. It is assumed that these would be physically close to their destination capillary bed, and would therefore have a small arterial transit time from label location to image slice (indeed, they could be within the destination imaging voxel when they are labeled). So far, however, vsASL has not been widely adopted, for a variety of reasons. These include an SNR penalty since the method is based on saturation rather than inversion of spins (although approaches to improve SNR have recently been proposed[62,63]); also not all blood spins can be labeled (only those moving predominantly along the gradient direction of the velocity-selective preparation module); and the method can be confounded by diffusion and eddy current effects, making quantification challenging.[64,65] The preparation module can even be made more sophisticated by directly labeling spins on the basis of acceleration (deceleration), so-called accASL.[66]

Vessel-selective labeling

Whilst the techniques described above provide vital information on total blood flow to a given region, the relative contributions from different feeding arteries cannot be known. Normal-appearing perfusion could be the result of efficient collateral flow, masking the presence of underlying vascular disease. Variation in vascular territories across subjects can also lead to incorrect assignment of an infarct to a particular feeding artery.[67] The ability to separately image flow arising from different feeding arteries can help avoid these problems as well as improve kinetic model fitting in regions of mixed blood supply.[68] Additionally, knowledge of the arterial supply to lesions such as tumors or arteriovenous malformations can help in treatment planning.[69] Below, some of the different methods for obtaining vessel-selective information with ASL are explored.

Single artery selective methods

Early vessel-selective methods relied on restricting the region over which inversion of the blood water was achieved, either using a transmit coil to produce a limited excitation field,[70,71,72] or by using appropriately oriented labeling slabs.[73-76] These approaches allowed some vessel-selectivity, but accurate targeting was limited by the coil geometry and/or vascular anatomy. Repeated pencil beam 2D RF pulses to target specific arteries was also proposed,[77] although this has difficulties with achieving a well-defined bolus of labeled blood, and may partially label other arteries. Methods that continuously rotate the labeling plane can induce adiabatic inversion at a single point in space, with reduction in inversion efficiency away from this point,[78,79] thus providing the ability to target individual vessels.

Similar selective excitation approaches are possible using pCASL, where gradient blips (orthogonal to the main labeling gradient) are applied between consecutive RF pulses.[80,81] The blip direction is either rotated within the transverse plane[80,81] or is pseudo-randomized.[81] This leads to efficient labeling at only one location, whereas at other locations there is a phase mismatch, resulting in low labeling efficiency. In the control condition the RF phase is further modulated by 180° every other RF pulse. These techniques avoid the difficulties of the CASL techniques, but partial labeling of nearby arteries may sometimes lead to ambiguity in the source of the blood signal.[80-83] Reduction in the size of the labeling 'spot' by increasing the gradient blips can improve the vessel-selectivity, but is accompanied by a reduction in labeling efficiency.[81]

Single-artery selective methods have the advantage of being relatively straightforward to prescribe and post-process. However, 2*N* images must be acquired (label and control) to encode *N* arteries, but with only two images being used to calculate the signal from any given artery. Compared to non-selective ASL, where all 2*N* images contribute signal from that artery, the SNR efficiency is therefore substantially reduced.[83,84]

Vessel-encoded methods

In vessel-encoded ASL multiple arteries are labeled in different combinations across different images (Fig. 4), and the contribution of each artery to the resulting signal is 'decoded' in post-processing. Labeling subsets of arteries can be achieved using a PASL labeling slab[84,85] or by using a modified selective pCASL approach with an elliptical labeling spot.[86] Alternatively, transverse gradient blips can be applied between pCASL RF pulses in a consistent direction,[87] which creates a periodic modulation in inversion efficiency along the specified axis. It is this latter method that has been the focus of most development and perhaps offers the greatest potential for clinical deployment.

Using a limited number of encoding steps and a simple series of additions and subtractions[85,86] or clustering methods,[88,89] it is possible to isolate the signals from different feeding arteries. However, these simple approaches implicitly assume that voxels do not receive blood supply from multiple feeding arteries, limiting their use in clinical scenarios where overlapping vascular territories may be present.

If the number of encodings equals or exceeds the number of arteries (plus static tissue) then the separate arterial signals can be recovered by constructing an encoding matrix, then taking the (pseudo)inverse, and applying it to the acquired images.[87,90,91] With this approach, if the encoding matrix corresponds to a Hadamard-type encoding then the SNR efficiency is equivalent to conventional ASL, even allowing for overlapping vascular territories.[84,87] This has been demonstrated experimentally, showing equivalence of CBF estimation[68] and negligible labeling of nearby arteries,[92] giving this method a considerable advantage over single-artery selective techniques where multiple arteries are of interest.

Nevertheless, to be successful all vessels within the labeling plane must be encoded, making irregular arrangements or large numbers of arteries more challenging. One solution is to use many 'random' encodings.[93] This avoids the need for careful planning, although large numbers of encodings may not be feasible for angiographic applications and SNR efficiency is expected to fall by a factor of $\sim\sqrt{2}$. Encodings can also be calculated using a Fourier-based technique, giving a minimal number of encoding cycles that closely approximate an ideal (Hadamard) scheme.[94] However, for applications where only a small subset of arteries within the labeling plane are of interest and/or SNR efficiency is not a primary concern, single-artery selective methods may be faster and simpler to perform.

[INSERT FIGURE 4 ABOUT HERE]

Kinetic Modeling

Perfusion quantification relies on a description of labeled blood water delivery to the voxel, and traditionally this has been based on the theory of tracer kinetics. The most general description of the kinetic model for ASL data was provided by Buxton et al.,[52] building on the previous modified Bloch equation formalism introduced by Williams et al.[18] Following the principles taken originally by Kety,[95] they described the signal arising from labeled water within a voxel as the convolution of an arterial input function and a residue function:

$$\Delta M(t) = 2\alpha M_{0b} f \int_0^t C(t')R(t-t')dt' = 2M_{0b} f . C(t) * R(t)$$

Where ΔM is the time series of (inverted) magnetization delivered to the voxel, M_{0b} is the equilibrium magnetization of the arterial blood, α is the inversion efficiency, and f is the perfusion (in units of s^{-1}). Methods for estimating M_{0b} and α are discussed below, the only other key information needed for quantification are descriptions of the arterial input function (AIF), $C(t)$, and the residue function, $R(t)$.

Arterial input function

It is normally assumed that the ASL labeling process creates a well-defined bolus of labeled blood water in the labeling region. This travels to the brain accumulating a delay: the 'arterial transit time', during which the label decays with the T1 of the blood. This gives rise to the major difference between pCASL and PASL labeling as seen in Fig. 5, the overall effect being that a higher signal is theoretically available from pCASL due to the availability of a larger total inverted magnetization that can be delivered. Additionally, dependent upon the acquisition, the AIF bolus duration may be unknown *a priori* for PASL, motivating the QUIPSS-based modifications discussed above.

Residue function

The residue function describes what happens to the labeled blood water once it has arrived in the voxel: for a unit of labelled water spins, it quantifies the quantity that remains. Thus, it starts at unity at time zero and decreases monotonically thereafter, reflecting the fact that label is gradually being lost. The dominant process that reduces the label is further T1 decay of the inverted spins. The residue function may be separated into two components: $R(t) = m(t).r(t)$. Where $m(t)$ represents the T1 decay and $r(t)$ captures other physical effects such a clearance of label into the venous vasculature.

[INSERT FIGURE 5 ABOUT HERE]

The simple model

The simplest model for the quantification of ASL perfusion, as advocated in the consensus paper by the ISMRM Perfusion Study Group and the European Consortium for ASL in Dementia,[29] assumes that all label arriving in the voxel remains there. This presumes that the majority of labeled blood water exchanges rapidly from the blood compartment into tissue, and clearance of label directly through the vasculature or via back-exchange from tissue to blood is negligible. The simple model also assumes that the T1 decay of label in tissue and arterial blood is the same.

The standard model

Earlier ASL kinetic models[53,96] made fewer simplifying assumptions, as captured in the work of Buxton et al.[52] In this 'standard' model a different (lower) T1 of tissue relative to blood was assumed, and clearance of labeled blood water to the venous circulation occurred at a rate determined by the perfusion and the equilibrium tissue/blood partition coefficient.

Dispersion

As noted by Buxton,[52] the complete delivery of blood to the voxel may occur with a range of arterial transit times, causing smoothing of the arterial input function. This could arise from the flow profile within the arteries and the effect of label arriving via different vascular paths, the overall effect being described as dispersion. A number of models have been proposed to account for dispersion effects, including use of a vascular transport function,[97,98] or by modeling dispersion from an assumed flow profile and vascular geometry.[99,100] These refinements are, however, rarely used in the process of quantification.

Exchange

A central assumption of the standard models is that labeled water remains almost entirely in the voxel, treating the voxel as a single well-mixed compartment. In practice this assumes high permeability of the vascular walls to water so that the labeled water exchanges into tissue where it will remain for the duration of the volume acquisition. Various models have been proposed that include an exchange process via two compartments separating capillary blood and extravascular space.[101-103] However, hindrances to water exchange are not readily observable from ASL data since effects rely on T1 differences between blood and tissue, which are not sufficiently large. A number of techniques have been explored that attempt to enhance the effect, allowing permeability to be measured, for example by using diffusion weighting (akin to flow suppression)[104,105] or via T2 measurements.[106-108]

Macrovascular component

Whilst possible to mitigate contamination from labeled blood water within large arteries through application of flow-crushing gradients during the readout,[109] the additional gradients necessitate longer echo times, thus reducing SNR, and only magnetisation flowing in the same direction as the crusher gradients is dephased, potentially leaving significant macrovascular signal.[110] An alternative is to incorporate macrovascular effects into the model. A separate component can be included that follows the form of the AIF, scaled by the arterial blood volume, to represent signals arising from the macrovasculature. This has been used to separate the macrovascular contribution in multi-delay PASL data,[110] where a residual macrovascular component was observed even after readout-based flow suppression. In practice, the macrovascular component will exhibit dispersion, whose effect is more noticeable than dispersion effects in the tissue signal.[98] This has been exploited to measure the local AIF by using a combination of flow-suppressed and non-suppressed data.[56]

Model inversion

The simple model affords an analytical relationship between ASL difference signal and perfusion that can be inverted for single post-label delay perfusion quantification.[29] Multi-delay data allows measurement and correction for the arterial transit time by fitting a kinetic model to the data, for example using non-linear fitting methods.

Bayesian model inversion has also been proposed, that permits incorporation of prior information about the model parameters, improving robustness in the face of the low SNR commonly seen with ASL.[111,112] Alternatively, a 'model-free' deconvolution analysis can be used for ASL data (similar to that used dynamic susceptibility contrast perfusion MRI analysis) if separate information about the AIF can be obtained.[56] Comparisons with model-based analyses[56,113] suggest that, as in other perfusion modalities, the 'model-free' methods tend to underestimate perfusion.[114]

Quantification and Calibration

The attraction of ASL is that it is theoretically a quantitative method, yielding values in accepted units (ml blood/100g tissue/min, although strictly speaking the units measured are ml blood/100ml tissue/min – a conversion to standard accepted units can be made if a value for tissue density is used). To obtain truly quantitative numbers there are, however, some caveats. One is that the inversion efficiency must either be assumed, or must be calibrated.[115,116] In practice the value is not measured in individual subjects, but rather a sensible estimate is used. Theory and experiments have shown that values of 85%-98% can be used, depending on the ASL technique.[29]

Another factor in quantification is the need to reference the signal differences measured in the ASL experiment to a normalization factor. Ideally this normalization should be against a voxel of fully relaxed blood, but this is not practically possible. Some studies have advocated a CSF-filled voxel for normalization, although this approach requires further correction for the bias field of the receive RF coil(s) and factors to account for differences in the T2 and proton density between blood and CSF. As such, an expedient strategy is to simply use a proton-density image, slightly blurred to account for possible mis-registration. This consists of an image acquired under full T1 relaxation conditions (long TR) and minimal T2 weighting (minimum TE), having the benefit of accounting for the receive coil bias, and also ensuring that the reference image is well registered to the ASL data if the same readout sequence is used. However, care should be taken to minimize noise propagation and edge/partial volume effects. A correction should also be made to account for the brain-blood partition coefficient of water (along with a caution that its value may not be truly constant across the brain).

In addition to determining the factors directly appearing in the equation relating the ASL signal to tissue perfusion (see above), there are a number of other artifacts and physiological effects that can hamper accurate quantification. Magnetic field inhomogeneity induces signal dropout and distortion or blurring artifacts in many commonly used readout schemes, leading to loss or mis-localization of the perfusion signal. Shorter echo times and spin-echo readout can reduce signal dropout, although more robust readout methods may be necessary to improve image quality at higher field.[117,118] Static field inhomogeneity can also be problematic for pCASL labeling, since it relies on particular increments in the phase of the magnetization between RF pulses. A number of approaches have been proposed to counter such effects, including measurement of the ASL signal at a range of RF phase increments[32] or by using pre-scans to estimate and correct for field offsets at the labeling plane.[33,119,120]

Attempts to validate the quantitative capability of ASL against the accepted gold standard of 15-oxygen PET have shown a good agreement, especially when the interval

between ASL and PET measurements is minimized.[121] However, some biases have been observed between different acquisition approaches, with the recommended approach of pCASL often showing an over-estimation of perfusion relative to PET. The recent availability of combined PET-MR scanners will hopefully allow more direct validations in patients to be made.

Partial Volume Effects

The central assumption of perfusion quantification using ASL is that we are measuring the delivery of blood to the capillary bed and thus a property of the tissue. It is also assumed that the tissue within a voxel can be treated as a single homogenous unit for which it is valid to quote a single perfusion value. Where a voxel contains a mixture of tissues with different perfusion properties, the measured value will be a weighted mean of those contributions. This is particularly common in the brain where voxels are likely to contain a mixture of grey matter, white matter and cerebrospinal fluid (CSF). CSF should contribute no ASL perfusion signal, and white matter has substantially lower perfusion than grey matter. Additionally, the longer arterial transit times observed in white matter may further lower the signal from white matter.

This has important implications when quoting mean grey matter perfusion values, as is common in the literature. The resolution of typical ASL data (~3 mm voxel dimensions) makes it almost impossible to find voxels with 100% grey matter in the perfusion image. Thus, a grey matter mask must be defined at a much lower threshold, including partial voluming with both WM and CSF in the final calculation, potentially explaining why quoted GM perfusion values from large studies[122] are in the range 30 – 40 ml/100g/min despite the accepted value of GM perfusion being closer to 60 ml/100g/min.

Several approaches have been proposed to correct for partial volume effects using independently derived estimates of the different tissues. The simplest approaches fix the ratio of GM to WM perfusion,[123] albeit unlikely to be constant everywhere in the healthy brain, let alone in disease. An alternative method used a linear regression-based approach that simultaneously estimates the GM and WM perfusion contributions in a voxel using information from local groups of voxels within a spatial region of predefined size.[124] A disadvantage of this approach is the degree of spatial smoothing introduced into the final perfusion images. Further refinements have been introduced to increase the robustness and limit spatial smoothing.[125] Additionally, spatial priors within a Bayesian model fitting method have been exploited to achieve partial volume correction in multi-delay ASL data[126] showing better preservation of detail than linear regression methods. Figure 6 illustrates the result of various correction methods.

[INSERT FIGURE 6 ABOUT HERE]

ASL Angiography

Rather than using a long post-labeling delay to visualize tissue perfusion, images can also be acquired soon after an ASL preparation while the labeled blood is still within the arteries, giving angiographic contrast. Indeed, some of the earliest examples of ASL were angiographic.[17,127,128] These images give crucial information about the structure and function of the arterial system, such as the presence of stenoses or occlusions,

without venous contamination that can be present in contrast-enhanced methods. As with all ASL techniques, static tissue is subtracted out, preventing it from obscuring smaller or lower contrast vessels, and allowing rapid 2D projection acquisitions without overlying tissue signal and partial volume effects. The high concentration of labeled blood within arterial voxels, and the minimal time delay between labeling and imaging, has the result that the SNR of ASL angiography is considerably higher than that of ASL perfusion imaging, important since higher spatial and temporal resolution are required to accurately delineate small vascular structures and dynamics of blood flow that occur within arteries.

Labeling approaches

As with perfusion imaging, any ASL preparation can be used with an angiographic readout, including CASL,[17] PASL[127,129,130] and pCASL.[131] Single-artery-selective[74,82,132-134] and vessel-encoded[92,135] preparations can also be used to produce vessel-selective angiograms similar to invasive x-ray digital subtraction angiography (see Fig. 7). Velocity- or acceleration-selective ASL angiograms have also been proposed.[136-138] The choice of the optimal labeling scheme depends somewhat on the intended application.

[INSERT FIGURE 7 ABOUT HERE]

For static angiography, in which a single image of the arterial system is desired, a PASL preparation can be used with the inversion time chosen to allow sufficient delay for labeled blood to enter the imaging region before image acquisition.[127] Alternatively, sufficiently long pCASL labeling[139] or hybrid approaches[82,131,140] can be applied to fill the vasculature with labeled blood. Velocity- or acceleration-selective preparations potentially eliminate delayed transit artifacts,[136-138] but suffer from reduced SNR and inefficient labeling of blood flowing orthogonally to the applied labeling gradients.[136]

Dynamic (time-resolved) angiograms give both anatomical and hemodynamic information that may be of additional clinical benefit,[141] and are shown schematically in Fig. 8. One advantage of PASL in this context is the ability to start imaging soon after labeling, such that inflow of the labeled blood can be visualized with a time-resolved readout.[129,130,142] In the case of pCASL the arterial system can be filled with labeled blood prior to image acquisition. However, timing information can still be extracted by observing the outflow of the blood.[135] Indeed, 'inflow subtraction' can be used to give the appearance of inflow rather than outflow,[92,143,144] or can be simulated after fitting a kinetic model.[145] Another approach relies on varying the labeling duration to build up a series of images showing wash-in of the labeled blood.[82,146]

[INSERT FIGURE 8 ABOUT HERE]

Readouts

In contrast to perfusion imaging, angiographic readouts typically acquire a single line of *k*-space (i.e., only a subset of the data needed to reconstruct an image) following each excitation pulse to minimize signal loss from flowing spins and to enable higher spatial resolution. Multiple lines of *k*-space can be acquired after each ASL preparation to reduce scan time, although too wide an acquisition window risks significant motion of the bolus of labeled blood during imaging, resulting in artifact. Staggered acquisition of

the same lines of *k*-space after each ASL preparation allows time-resolved images to be reconstructed (see Figure 8).

ASL angiography has been demonstrated with various fast gradient-echo MRI sequences (including balanced steady-state free precession, bSSFP,[140,147-150] and spoiled gradient echo, SPGR[130,131,133-135,142,144]). Of these readout methods bSSFP is considerably more SNR efficient, since transverse magnetization is recycled from one excitation to the next.[30] However, it suffers from signal loss in regions with poor magnetic field homogeneity,[92,151] limiting its use at higher field strengths and over larger fields of view. SPGR does not suffer from these artifacts and may provide more accurate depiction of stenoses,[152] but each excitation pulse destroys some of the remaining ASL signal, limiting the flip angle and TR that can be used and thus its SNR efficiency. The choice of the optimal readout scheme is therefore likely to be application dependent.

Another challenge of time-resolved 3D angiography is its acquisition time due to the high spatial and temporal resolution required. As well as conventional acceleration techniques such as parallel imaging,[153,154] the relatively high SNR and sparsity of angiographic images make them suitable for undersampled non-Cartesian trajectories, which have shown excellent image quality and a considerable scan time saving whilst maintaining high isotropic resolution.[131,140,146] Reduced sensitivity to motion artifacts and improved vessel delineation has also been demonstrated in coronary angiography.[155]

Modeling and quantification

Despite using an identical preparation, angiographic signal evolution differs considerably from the standard Buxton model (described above). Specifically, blood does not accumulate in the arteries as it does in tissue, so the signal intensity depends mostly on arterial blood volume rather than blood flow. The PASL signal can be described empirically with a gamma function,[141] and a pCASL model that including the effects of dispersion, T1 decay and attenuation has also been proposed.[145] The model fits provide useful markers of disease but do not provide direct measures of blood flow through the arterial system. However, such estimates may be derived from signals summed across an arterial region of interest, either by comparison with a separately measured arterial input function[132] or by fitting a kinetic model extrapolated to a very short labeling duration.[156] More work is required in this area to further validate and improve the robustness of such methods.

Applications of ASL

ASL has been deployed as a tool in basic research studies since its earliest days, but its clinical impact has been rather modest, largely due to the delay in its appearance on clinical scanners. Now that ASL is available on clinical scanners,[157] and there are clearer consensus protocols agreed, its use is growing, further prompted by the increasing move away from gadolinium-based contrast agent approaches.[158] Due to its non-invasive nature, ASL offers the benefit over competitor methods of being able to be used in longitudinal assessment of perfusion or vessel status, as well as in patients who are contraindicated for gadolinium-based contrast agents. This makes ASL an attractive candidate for monitoring disease progression or treatment response, since regular non-invasive measurements are possible.

One use of ASL has been in the study of brain function, analogous to blood-oxygenation level-dependent (BOLD) functional MRI. In some circumstances ASL-based fMRI is preferred over BOLD-based fMRI, despite its poorer SNR, especially for task paradigms longer than a few minutes[159] (e.g. in the study of tonic pain[160]), or where only minimal task cycling is possible (such as pharmacological studies where only a single transition in neurological state may be possible). The ability of ASL to withstand long or sparse paradigms is due to its subtractive nature, making it insensitive to slow signal drifts that affect BOLD data. Perfusion measurement is also a key component of MRI methods seeking to measure the metabolic rate of oxygen consumption ($CMRO_2$) using hypercapnia or hyperoxia to induce flow or metabolic changes, and can also offer a measure of cerebrovascular reserve in response to a blood flow challenge.[161,162]

[INSERT FIGURE 9 ABOUT HERE]

Clinically, ASL has mainly been used in the assessment of cerebrovascular disease. The principal areas have been in stroke,[163-165] steno-occlusive disease,[166,167] arteriovenous malformation,[168,169] and Moyamoya disease.[170-171] A number of studies have used ASL in the characterization of dementia (including Alzheimer's disease,[172,173] and vascular dementia[174,175]). In Alzheimer's disease, ASL has shown similar patterns of hypo-perfusion to FDG-PET, suggesting that it can be used in place of PET for metabolic assessment. Differences in perfusion patterns have also been observed between Alzheimer's patients and fronto-temporal dementia.[176] An example of application of ASL to steno-occlusive disease is shown in Fig. 9, demonstrating evidence of collateral flow compensating for disrupted blood supply through one of the proximal arteries in a patient suffering from transient ischemic attack. Another example application to cerebrovascular disease is shown in Fig. 10, demonstrating ASL's potential in characterization of arteriovenous malformations. In this case vessel-selective ASL angiography was used to visualize arterial branches supplying the AVM, with relevance to pre-intervention assessment.

[INSERT FIGURE 10 ABOUT HERE]

ASL has also been deployed extensively in neuro-oncology, both to aid diagnosis[177-178] and therapy monitoring,[179] and to assist pre-surgical planning.[180] Higher grade tumours tend to show higher perfusion and vascularity, and ASL is also able to help distinguish tumourous progression from contrast-enhancing mimics and radiation necrosis. ASL has also found application in epilepsy[181-182] to aid detection of epileptogenic focus by monitoring peri-ictal CBF increases. There is also hope that ASL will have a role in multiple sclerosis,[183-185] where correlations have been found between ASL measures and lesion burden and disability. Another emerging use is in head trauma,[186] where ASL has shown specific patterns of perfusion abnormality. This includes the category of mild traumatic brain injury (e.g. following concussion) where structural changes may be too subtle to measure, but CBF changes can be detected. Finally, ASL has been used to study a number of mental health disorders, predominantly depression,[187] schizophrenia,[188] and post-traumatic stress disorder.[189] Patterns of hypoperfusion have been seen in frontal areas in depressed patients, along with hypoperfusion in regions associated with the default mode network. In post-traumatic stress disorder, regions of elevated CBF in parietal and temporal cortices have been found.

Conclusions

ASL is now a well-established MRI method for assessing cerebral perfusion in a quantitative manner. However, due to its complexity, challenging SNR characteristics, and slow translation into a clinically available tool, it has still not realized the impact that it promises. Now that there is a growing consensus on the imaging strategies and analysis methods to use, it is likely to become an increasingly valuable tool in the armoury of MRI methods, with utility in a variety of neurological and psychiatric diseases. Its ability to map the large vessels in an angiographic mode, with an associated improvement in signal-to-noise due to the improved partial volume fraction, also offers an exciting new tool for non-invasive assessment of the cerebrovasculature. By adding specificity to the arterial labeling it should see application in collateral flow assessment, intervention planning for arteriovenous malformation treatment, and possibly also tumour surgery planning.

Acknowledgements: We thank the Dunhill Medical Trust (grant OSRP1/1006), the EPSRC (grant EP/P012361/1) and the Royal Academy of Engineering (TWO). We also acknowledge our clinical collaborators, Dr Ursula Schulz and Dr Natalie Voets, and the facilities provided by the Oxford Acute Vascular Imaging Centre. The Wellcome Centre for Integrative Neuroimaging is supported by core funding from the Wellcome Trust (203139/Z/16/Z).

Disclosures: The authors hold patents on perfusion and angiography analysis methods that have been licensed to Siemens Healthineers.

References

1 Gullberg GT, Wehrli FW, Shimakawa A, Simons MA. MR vascular imaging with a fast gradient refocusing pulse sequence and reformatted images from transaxial sections. *Radiology* 1987; **165**: 241–6.

2 Moran PR. A flow velocity zeugmatographic interlace for NMR imaging in humans. *Magn Reson Imaging* 1982; **1**: 197–203.

3 Gur D, Good WF, Wolfson SK, Yonas H, Shabason L. In vivo mapping of loca cerebral blood flow by xenon-enhanced computed tomography. *Science* 1982; **215**:1267-1268.

4 Herscovitch P, Markham J, Raichle ME. Brain blood flow measured with intravenous H2(15)O. I. Theory and error analysis. *J Nucl Med* 1983; **24**:782-789.

5 Raichle ME, Martin WR, Herscovitch P, Mintum MA, Markham J. Brain blood flow measured with intravenous H2(15)O. II. Implementation nd validation. *J Nucl Med* 1983; **24**:790-798.

6 Le Bihan D, Breton E, Lallemand D, Grenier P, Cabanis E, Laval-Jeantet M. MR imaging of intravoxel incoherent motions: application to diffusion and perfusion in neurologic disorders. *Radiology* 1986; **161**: 401–407.

7 Villringer A, Rosen BR, Belliveau JW, Ackerman JL, Lauffer RB, Buxton RB *et al.* Dynamic imaging with lanthanide chelates in normal brain: Contrast due to magnetic susceptibility effects. *Magn Reson Med* 1988; **6**: 164–174.

8 Rosen BR, Belliveau JW, Vevea JM, Brady TJ. Perfusion imaging with NMR contrast agents. *Magn Reson Med* 1990; **14**: 249–265.

9 Calamante F, Gadian DG, Connelly A. Delay and dispersion effects in dynamic susceptibility contrast MRI: simulations using singular value decomposition. *Magn Reson Med* 2000; **44**:466–73

10 Calamante F, Gadian DG, Connelly A. Quantification of perfusion using bolus tracking magnetic resonance imaging in stroke: assumptions, limitations, and potential implications for clinical use. *Stroke* 2002; **33**:1146-1151.

11 PekarJ, Ligeti L, Ruttner Z, Lyon RC, Sinnwell TM, van Gelderen P, Fiat D, Moonen CT, McLaughlin AC. In vivo measurement of cerebral oxygen consumption and blood flow using 17O magnetic resonance imaging. *Magn Reson Med* 1991; **21**:313-319.

12 Koretsky AP. Early development of arterial spin labeling to measure regional brain blood flow by MRI. *Neuroimage* 2012; **62**: 602–607.

13 Singer JR. Blood flow rates by nuclear magnetic resonance measurements. *Science* 1959; **130**:1652-1653.

14 Ackerman JJ, Ewy CS, Kim SG, Shalwitz RA. Deuterium magnetic resonance in vivo: the measurement of blood flow and tissue perfusion. *Ann NY Acad Sci* 1987; **508**:89–98.

15 Kim SG, Ackerman JJ. Quantitative determination of tumor blood flow and perfusion via deuterium nuclear magnetic resonance spectroscopy in mice. *Cancer Res* 1988; **48**:3449–3453.

16 Eleff SM, Schnall MD, Ligetti L, Osbakken M, Subramanian VH, Chance B, Leigh JS Jr. Concurrent measurements of cerebral blood flow, sodium, lactate, and high-energy phosphate metabolism using 19F, 23Na,1H, and 31P nuclear magnetic resonance spectroscopy. *Magn Reson Med* 1988; **7**:412–424.

17 Dixon WT, Du LN, Faul DD, Gado M, Rossnick S. Projection angiograms of blood labeled by adiabatic fast passage. *Magn Reson Med* 1986; **3**: 454–462.

18 Williams DS, Detre JA, Leigh JS, Koretsky AP. Magnetic resonance imaging of

perfusion using spin inversion of arterial water. *Proc Natl Acad Sci U S A* 1992; **89**: 212–6.

19 Detre JA, Leigh JS, Williams DS, Koretsky AP. Perfusion imaging. *Magn Reson Med* 1992; **23**: 37–45.

20 Roberts DA, Detre JA, Bolinger L, Insko EK, Leigh JS. Quantitative magnetic resonance imaging of human brain perfusion at 1.5 T using steady-state inversion of arterial water. *Proc Natl Acad Sci* 1994; **91**: 33–37.

21 Edelman RR, Siewert B, Darby DG, Thangaraj V, Nobre a C, Mesulam MM *et al.* Qualitative mapping of cerebral blood flow and functional localization with echo-planar MR imaging and signal targeting with alternating radio frequency. *Radiology* 1994; **192**: 513–520.

22 Wong EC, Buxton RB, Frank LR. Implementation of quantitative perfusion imaging techniques for functional brain mapping using pulsed arterial spin labeling. *NMR Biomed* 1997; **10**: 237–249.

23 Kwong KK, Belliveau JW, Chesler DA, Goldberg IE, Weisskoff RM, Poncelet BP, Kennedy DN, Hoppel BE, Cohen MS, Turner R et al. Dynamic magnetic resonance imaging of human brain activity during primary sensory stimulation. *Proc Natl Acad Sci USA* 1992; **89**:5675-5679.

24 Kim S-G. Quantification of relative cerebral blood flow change by flow-sensitive alternating inversion recovery (FAIR) technique: Application to functional mapping. *Magn Reson Med* 1995; **34**: 293–301.

25 Kwong KK, Chesler DA, Weisskoff RM, Donahue KM, Davis TL, Ostergaard L *et al.* MR perfusion studies with T1-weighted echo planar imaging. *Magn Reson Med* 1995; **34**: 878–87.

26 Wolff SD, Balaban RS. Magnetization transfer contrast (MTC) and tissue water proton relaxation in vivo. *Magn Reson Med* 1989; **10**: 135–144.

27 Alsop DC, Detre J a. Multisection cerebral blood flow MR imaging with continuous arterial spin labeling. *Radiology* 1998; **208**: 410–416.

28 Dai W, Garcia D, de Bazelaire C, Alsop DC. Continuous flow-driven inversion for arterial spin labeling using pulsed radio frequency and gradient fields. *Magn Reson Med* 2008; **60**: 1488–1497.

29 Alsop DC, Detre JA, Golay X, Günther M, Hendrikse J, Hernandez-Garcia L *et al.* Recommended implementation of Arterial Spin-Labeled perfusion MRI for clinical applications: A consensus of the ISMRM Perfusion Study group and the European consortium for ASL in dementia. *Magn Reson Med* 2015; **73**: 102–116.

30 Scheffler K, Lehnhardt S. Principles and applications of balanced SSFP techniques. *Eur Radiol* 2003; **13**: 2409–2418.

31 Garcia DM, de Bazelaire C, Alsop D. Pseudo-continuous Flow Driven Adiabatic Inversion for Arterial Spin Labeling. In: *Proceedings of the 13th Annual Meeting of ISMRM*. Miami, USA, 2005, p 37.

32 Jung Y, Wong EC, Liu TT. Multiphase pseudocontinuous arterial spin labeling (MP-PCASL) for robust quantification of cerebral blood flow. *Magn Reson Med* 2010; **64**: 799–810.

33 Luh WM, Talagala SL, Li TQ, Bandettini PA. Pseudo-continuous arterial spin labeling at 7 T for human brain: Estimation and correction for off-resonance effects using a Prescan. *Magn Reson Med* 2013; **69**: 402–410.

34 Maccotta L, Detre JA, Alsop DC. The efficiency of adiabatic inversion for perfusion imaging by arterial spin labeling. *NMR Biomed* 1997; **10**: 216–221.

35 Silva AC, Zhang W, Williams DS, Koretsky AP. Multi-Slice MRI of Rat Brain

Perfusion During Amphetamine Stimulation Using Arterial Spin Labeling. *Magn Reson Med* 1995; **33**: 209–214.
36 Zaharchuk G, Ledden PJ, Kwong KK, Reese TG, Rosen BR, Wald LL. Multislice perfusion and perfusion territory imaging in humans with separate label and image coils. *Magn Reson Med* 1999; **41**: 1093–1098.
37 Wong EC, Buxton RB, Frank LR. Quantitative imaging of perfusion using a single subtraction (QUIPSS and QUIPSS II). *Magn Reson Med* 1998; **39**: 702–708.
38 Mansfield P. Multi-planar image formation using NMR spin echoes. *J Phys C Solid State Phys* 1977; **10**: L55–L58.
39 Duhamel G, Alsop DC. Single-shot susceptibility insensitive whole brain 3D fMRI with ASL. In: *Proceedings of the 12th Annual Meeting of ISMRM*. Kyoto, Japan, 2004, p 518.
40 Feinberg DA, Oshio K. GRASE (gradient- and spin-echo) MR imaging: a new fast clinical imaging technique. *Radiology* 1991; **181**: 597–602.
41 Günther M, Oshio K, Feinberg DA. Single-shot 3D imaging techniques improve arterial spin labeling perfusion measurements. *Magn Reson Med* 2005; **54**: 491–498.
42 Dixon WT, Sardashti M, Castillo M, Stomp GP. Multiple inversion recovery reduces static tissue signals in angiograms. *Magn Reson Med* 1991; **18**:257-268.
43 Mani S, Pauly J, Conolly S, Meyer C, Nishimura D. Background suppression with multiple inversion recovery nulling: applications to projective angiography. *Magn Reson Med* 1997; **37**:898-905.
44 Ye FQ, Frank JA, Weinberger DR, McLaughlin AC. Noise reduction in 3D perfusion imaging by attenuating the static signal in arterial spin tagging (ASSIST). *Magn Reson Med* 2000; **44**: 92–100.
45 Zun Z, Shankaranarayanan A, Zaharchuk G. Pseudocontinuous arterial spin labeling with prospective motion correction (PCASL-PROMO). *Magn Reson Med* 2014; **72**: 1049–1056.
46 Frost R, Hess AT, Okell TW, Chappell MA, Tisdall MD, van der Kouwe AJW *et al.* Prospective motion correction and selective reacquisition using volumetric navigators for vessel-encoded arterial spin labeling dynamic angiography. *Magn Reson Med* 2016; **76**: 1420–1430.
47 Wang Z, Aguirre GK, Rao H, Wang J, Fernández-Seara MA, Childress AR *et al.* Empirical optimization of ASL data analysis using an ASL data processing toolbox: ASLtbx. *Magn Reson Imaging* 2008; **26**: 261–269.
48 Tan H, Maldjian JA, Pollock JM, Burdette JH, Yang LY, Deibler AR *et al.* A fast, effective filtering method for improving clinical pulsed arterial spin labeling MRI. *J Magn Reson Imaging* 2009; **29**: 1134–1139.
49 Wang Z. Improving cerebral blood flow quantification for arterial spin labeled perfusion MRI by removing residual motion artifacts and global signal fluctuations. *Magn Reson Imaging* 2012; **30**: 1409–1415.
50 Fazlollahi A, Bourgeat P, Liang X, Meriaudeau F, Connelly A, Salvado O *et al.* Reproducibility of multiphase pseudo-continuous arterial spin labeling and the effect of post-processing analysis methods. *Neuroimage* 2015; **117**: 191–201.
51 van Osch MJ, Teeuwisse WM, Chen Z, Suzuki Y, Helle M, Schmid S. Advances in arterial spin labelling MRI methods for measuring perfusion and collateral flow. *J Cereb Blood Flow Metab* 2017; **In Press**: DOI: 10.1177/0271678X17713434.
52 Buxton RB, Frank LR, Wong EC, Siewert B, Warach S, Edelman RR. A general kinetic model for quantitative perfusion imaging with arterial spin labeling. *Magn*

Reson Med 1998; **40**: 383–396.
53 Alsop DC, Detre JA. Reduced Transit-Time Sensitivity in Noninvasive Magnetic Resonance Imaging of Human Cerebral Blood Flow. *J Cereb Blood Flow Metab* 1996; **16**: 1236–1249.
54 Look DC, Locker DR. Time Saving in Measurement of NMR and EPR Relaxation Times. *Rev Sci Instrum* 1970; **41**: 250–251.
55 Günther M, Bock M, Schad LR. Arterial spin labeling in combination with a look-locker sampling strategy: Inflow turbo-sampling EPI-FAIR (ITS-FAIR). *Magn Reson Med* 2001; **46**: 974–984.
56 Petersen ET, Lim T, Golay X. Model-free arterial spin labeling quantification approach for perfusion MRI. *Magn Reson Med* 2006; **55**: 219–232.
57 Günther M. Highly efficient accelerated acquisition of perfusion inflow series by cycled arterial spin labeling. In: *Proceedings of the 16th Annual Meeting of ISMRM*. Berlin, Germany, 2007, p 380.
58 Wells JA, Lythgoe MF, Gadian DG, Ordidge RJ, Thomas DL. In vivo Hadamard encoded continuous arterial spin labeling (H-CASL). *Magn Reson Med* 2010; **63**: 1111–1118.
59 Dai W, Shankaranarayanan A, Alsop DC. Volumetric measurement of perfusion and arterial transit delay using hadamard encoded continuous arterial spin labeling. *Magn Reson Med* 2013; **69**: 1014–1022.
60 Teeuwisse WM, Schmid S, Ghariq E, Veer IM, van Osch MJP. Time-encoded pseudocontinuous arterial spin labeling: basic properties and timing strategies for human applications. *Magn Reson Med* 2014; **72**: 1712–1722.
61 Wong EC, Cronin M, Wu W-C, Inglis B, Frank LR, Liu TT. Velocity-selective arterial spin labeling. *Magn Reson Med* 2006; **55**: 1334–1341.
62 Guo J, Wong EC. Increased SNR efficiency in velocity selective arterial spin labeling using multiple velocity selective saturation modules (mm-VSASL). *Magn Reson Med* 2015; **74**: 694–705.
63 Qin Q, van Zijl PCM. Velocity-selective-inversion prepared arterial spin labeling. *Magn Reson Med* 2016; **76**: 1136–1148.
64 Meakin JA, Jezzard P. An optimized velocity selective arterial spin labeling module with reduced eddy current sensitivity for improved perfusion quantification. *Magn Reson Med* 2013; **69**: 832–838.
65 Guo J, Meakin JA, Jezzard P, Wong EC. An optimized design to reduce eddy current sensitivity in velocity-selective arterial spin labeling using symmetric BIR-8 pulses. *Magn Reson Med* 2015; **73**: 1085–1094.
66 Schmid S, Ghariq E, Teeuwisse WM, Webb A, Van Osch MJP. Acceleration-selective arterial spin labeling. *Magn Reson Med* 2014; **71**: 191–199.
67 Hendrikse J, Petersen ET, Chèze A, Chng SM, Venketasubramanian N, Golay X. Relation between cerebral perfusion territories and location of cerebral infarcts. *Stroke* 2009; **40**: 1617–1622.
68 Okell TW, Chappell MA, Kelly ME, Jezzard P. Cerebral blood flow quantification using vessel-encoded arterial spin labeling. *J Cereb Blood Flow Metab* 2013; **33**: 1716–1724.
69 Helle M, Rüfer S, van Osch MJP, Nabavi A, Alfke K, Norris DG *et al.* Superselective arterial spin labeling applied for flow territory mapping in various cerebrovascular diseases. *J Magn Reson Imaging* 2013; **38**: 496–503.
70 Detre JA, Zhang W, Roberts DA, Silva AC, Williams DS, Grandis DJ *et al.* Tissue specific perfusion imaging using arterial spin labeling. *NMR Biomed* 1994; **7**: 75–

82.
71 Trampel R, Mildner T, Goerke U, Schaefer A, Driesel W, Norris DG. Continuous arterial spin labeling using a local magnetic field gradient coil. *Magn Reson Med* 2002; **48**: 543–546.
72 Werner R, Alfke K, Schaeffter T, Nabavi A, Mehdorn HM, Jansen O. Brain perfusion territory imaging applying oblique-plane arterial spin labeling with a standard send/receive head coil. *Magn Reson Med* 2004; **52**: 1443–1447.
73 Edelman RR, Mattle HP, O'Reilly G V, Wentz KU, Liu C, Zhao B. Magnetic resonance imaging of flow dynamics in the circle of Willis. *Stroke* 1990; **21**: 56–65.
74 Eastwood JD, Holder CA, Hudgins PA, Song AW. Magnetic resonance imaging with lateralized arterial spin labeling. *Magn Reson Imaging* 2002; **20**: 583–586.
75 Hendrikse J, van der Grond J, Lu H, Van Zijl PCM, Golay X. Flow territory mapping of the cerebral arteries with regional perfusion MRI. *Stroke* 2004; **35**: 882–887.
76 Golay X, Petersen ET, Hui F. Pulsed star labeling of arterial regions (PULSAR): a robust regional perfusion technique for high field imaging. *Magn Reson Med* 2005; **53**: 15–21.
77 Davies NP, Jezzard P. Selective arterial spin labeling (SASL): Perfusion territory mapping of selected feeding arteries tagged using two-dimensional radiofrequency pulses. *Magn Reson Med* 2003; **49**: 1133–1142.
78 Werner R, Norris DG, Alfke K, Mehdorn HM, Jansen O. Continuous artery-selective spin labeling (CASSL). *Magn Reson Med* 2005; **53**: 1006–1012.
79 Helle M, Rüfer S, Alfke K, Jansen O, Norris DG. Perfusion territory imaging of intracranial branching arteries - optimization of continuous artery-selective spin labeling (CASSL). *NMR Biomed* 2011; **24**: 404–412.
80 Dai W, Robson PM, Shankaranarayanan A, Alsop DC. Modified pulsed continuous arterial spin labeling for labeling of a single artery. *Magn Reson Med* 2010; **64**: 975–982.
81 Helle M, Norris DG, Rüfer S, Alfke K, Jansen O, van Osch MJP. Superselective pseudocontinuous arterial spin labeling. *Magn Reson Med* 2010; **64**: 777–786.
82 Robson PM, Dai W, Shankaranarayanan A, Rofsky NM, Alsop DC. Time-resolved Vessel-selective Digital Subtraction MR Angiography of the Cerebral Vasculature with Arterial Spin Labeling. *Radiology* 2010; **257**: 507–515.
83 Lindner T, Larsen N, Jansen O, Helle M. Accelerated visualization of selected intracranial arteries by cycled super-selective arterial spin labeling. *Magn Reson Mater Physics, Biol Med* 2016; **29**: 843–852.
84 Günther M. Efficient visualization of vascular territories in the human brain by cycled arterial spin labeling MRI. *Magn Reson Med* 2006; **56**: 671–675.
85 Zimine I, Petersen ET, Golay X. Dual vessel arterial spin labeling scheme for regional perfusion imaging. *Magn Reson Med* 2006; **56**: 1140–1144.
86 Helle M, Rüfer S, van Osch MJP, Jansen O, Norris DG. Selective multivessel labeling approach for perfusion territory imaging in pseudo-continuous arterial spin labeling. *Magn Reson Med* 2012; **68**: 214–219.
87 Wong EC. Vessel-Encoded Arterial Spin-Labeling Using Pseudocontinuous Tagging. *Magn Reson Med* 2007; **58**: 1086–1091.
88 Wong E, Kansagra A. Mapping Middle Cerebral Artery Branch Territories with Vessel Encoded Pseudo-Continuous ASL: Sine/Cosine Tag Modulation and Data Clustering in Tagging Efficiency Space. In: *Proceedings 16th Scientific Meeting of the ISMRM*. Toronto, Canada, 2008, p 182.
89 Gevers S, Bokkers RP, Hendrikse J, Majoie CB, Kies DA, Teeuwisse WM *et al.*

Robustness and reproducibility of flow territories defined by planning-free vessel-encoded pseudocontinuous arterial spin-labeling. *AJNR Am J Neuroradiol* 2012; **33**: E21-25.

90 Chappell MA, Okell TW, Jezzard P, Woolrich MW. A general framework for the analysis of vessel encoded arterial spin labeling for vascular territory mapping. *Magn Reson Med* 2010; **64**: 1529–1539.

91 Chappell MA, Okell TW, Payne SJ, Jezzard P, Woolrich MW. A fast analysis method for non-invasive imaging of blood flow in individual cerebral arteries using vessel-encoded arterial spin labelling angiography. *Med Image Anal* 2012; **16**: 831–839.

92 Okell TW, Schmitt P, Bi X, Chappell MA, Tijssen RHN, Sheerin F *et al.* Optimization of 4D vessel-selective arterial spin labeling angiography using balanced steady-state free precession and vessel-encoding. *NMR Biomed* 2016; **29**: 776–786.

93 Wong EC, Guo J. Blind detection of vascular sources and territories using random vessel encoded arterial spin labeling. *MAGMA* 2012; **25**: 95–101.

94 Berry ESK, Jezzard P, Okell TW. An Optimized Encoding Scheme for Planning Vessel-Encoded Pseudocontinuous Arterial Spin Labeling. *Magn Reson Med* 2015; **74**: 1248–56.

95 Kety SS, Schmidt CF. The Nitrous Oxide Method for the Quantitative Determination of Cerebral Blood Flow in Man: Theory, Procedure and Normal Values. *J Clin Invest* 1948; **27**: 476–483.

96 Calamante F, Williams SR, Van Bruggen N, Kwong KK, Turner R. A model for quantification of perfusion in pulsed labelling techniques. *NMR Biomed* 1996; **9**: 79–83.

97 Hrabe J, Lewis D. Two analytical solutions for a model of pulsed arterial spin labeling with randomized blood arrival times. *J Magn Reson* 2004; **167**: 49–55.

98 Chappell MA, Woolrich MW, Kazan S, Jezzard P, Payne SJ, MacIntosh BJ. Modeling dispersion in arterial spin labeling: Validation using dynamic angiographic measurements. *Magn Reson Med* 2013; **69**: 563–570.

99 Gallichan D, Jezzard P. Modeling the effects of dispersion and pulsatility of blood flow in pulsed arterial spin labeling. *Magn Reson Med* 2008; **60**: 53–63.

100 Kazan SM, Chappell MA, Payne SJ. Modeling the Effects of Flow Dispersion in Arterial Spin Labeling. *IEEE Trans Biomed Eng* 2009; **56**: 1635–1643.

101 Zhou J, Wilson D a, Ulatowski J a, Traystman RJ, van Zijl PCM. Two-Compartment Exchange Model for Perfusion Quantification Using Arterial Spin Tagging. *J Cereb Blood Flow Metab* 2001; **21**: 440–455.

102 St. Lawrence KS, Frank JA, McLaughlin AC. Effect of restricted water exchange on cerebral blood flow values calculated with arterial spin tagging: A theoretical investigation. *Magn Reson Med* 2000; **44**: 440–449.

103 Parkes LM, Tofts PS. Improved accuracy of human cerebral blood perfusion measurements using arterial spin labeling: Accounting for capillary water permeability. *Magn Reson Med* 2002; **48**: 27–41.

104 Wang J, Fernández-Seara MA, Wang S, Lawrence KSS. When Perfusion Meets Diffusion: in vivo Measurement of Water Permeability in Human Brain. *J Cereb Blood Flow Metab* 2007; **27**: 839–849.

105 St. Lawrence KS, Owen D, Wang DJJ. A two-stage approach for measuring vascular water exchange and arterial transit time by diffusion-weighted perfusion MRI. *Magn Reson Med* 2012; **67**: 1275–1284.

106 Gregori J, Schuff N, Kern R, Günther M. T2-based arterial spin labeling measurements of blood to tissue water transfer in human brain. *J Magn Reson*

Imaging 2013; **37**: 332–342.
107 Schmid S, Teeuwisse WM, Lu H, van Osch MJP. Time-efficient determination of spin compartments by time-encoded pCASL T2-relaxation-under-spin-tagging and its application in hemodynamic characterization of the cerebral border zones. *Neuroimage* 2015; **123**: 72–79.
108 Wells JA, Lythgoe MF, Choy M, Gadian DG, Ordidge RJ, Thomas DL. Characterizing the Origin of the Arterial Spin Labelling Signal in MRI Using a Multiecho Acquisition Approach. *J Cereb Blood Flow Metab* 2009; **29**: 1836–1845.
109 Ye FQ, Mattay VS, Jezzard P, Frank JA, Weinberger DR, McLaughlin AC. Correction for vascular artifacts in cerebral blood flow values measured by using arterial spin tagging techniques. *Magn Reson Med* 1997; **37**: 226–235.
110 Chappell MA, MacIntosh BJ, Donahue MJ, Günther M, Jezzard P, Woolrich MW. Separation of macrovascular signal in multi-inversion time arterial spin labelling MRI. *Magn Reson Med* 2010; **63**: 1357–1365.
111 Chappell MA, Groves AR, Whitcher B, Woolrich MW. Variational Bayesian Inference for a Nonlinear Forward Model. *IEEE Trans Signal Process* 2009; **57**: 223–236.
112 Groves AR, Chappell MA, Woolrich MW. Combined spatial and non-spatial prior for inference on MRI time-series. *Neuroimage* 2009; **45**: 795–809.
113 Chappell MA, Woolrich MW, Petersen ET, Golay X, Payne SJ. Comparing model-based and model-free analysis methods for QUASAR arterial spin labeling perfusion quantification. *Magn Reson Med* 2013; **69**: 1466–1475.
114 Østergaard L, Weisskoff RM, Chesler DA, Gyldensted C, Rosen BR. High resolution measurement of cerebral blood flow using intravascular tracer bolus passages. Part I: Mathematical approach and statistical analysis. *Magn Reson Med* 1996; **36**: 715–725.
115 Zhan W, Gu H, Silbersweig DA, Stern E, Yang Y. Inversion profiles of adiabatic inversion pulses for flowing spins: the effects on labeling efficiency and labeling accuracy in perfusion imaging with pulsed arterial spin-labeling. *Magn Reson Imaging* 2002; **20**: 487–494.
116 O'Gorman RL, Summers PE, Zelaya FO, Williams SCR, Alsop DC, Lythgoe DJ. In vivo estimation of the flow-driven adiabatic inversion efficiency for continuous arterial spin labeling: A method using phase contrast magnetic resonance angiography. *Magn Reson Med* 2006; **55**: 1291–1297.
117 Zuo Z, Wang R, Zhuo Y, Xue R, St Lawrence KS, Wang DJJ. Turbo-FLASH based arterial spin labeled perfusion MRI at 7 T. *PLoS One* 2013; **8**: e66612.
118 Wang Y, Moeller S, Li X, Vu AT, Krasileva K, Ugurbil K *et al.* Simultaneous multi-slice Turbo-FLASH imaging with CAIPIRINHA for whole brain distortion-free pseudo-continuous arterial spin labeling at 3 and 7 T. *Neuroimage* 2015; **113**: 279–288.
119 Jahanian H, Noll DC, Hernandez-Garcia L. B0 field inhomogeneity considerations in pseudo-continuous arterial spin labeling (pCASL): effects on tagging efficiency and correction strategy. *NMR Biomed* 2011; **24**: 1202–1209.
120 Shin DD, Liu TT, Wong EC, Shankaranarayanan A, Jung Y. Pseudocontinuous arterial spin labeling with optimized tagging efficiency. *Magn Reson Med* 2012; **68**: 1135–1144.
121 Fan AP, Jahanian H, Holdsworth SJ, Zaharchuk G. Comparison of cerebral blood flow measurement with 15O-water positron emission tomography and arterial spin labeling magnetic resonance imaging: a systematic review. *J Cereb Blood Flow*

Metab 2016; **36**:842-861.

122 Petersen ET, Mouridsen K, Golay X. The QUASAR reproducibility study, Part II: Results from a multi-center Arterial Spin Labeling test-retest study. *Neuroimage* 2010; **49**: 104–113.

123 Johnson NA, Jahng G-H, Weiner MW, Miller BL, Chui HC, Jagust WJ *et al.* Pattern of Cerebral Hypoperfusion in Alzheimer Disease and Mild Cognitive Impairment Measured with Arterial Spin-labeling MR Imaging: Initial Experience. *Radiology* 2005; **234**: 851–859.

124 Asllani I, Borogovac A, Brown TR. Regression algorithm correcting for partial volume effects in arterial spin labeling MRI. *Magn Reson Med* 2008; **60**: 1362–1371.

125 Liang X, Connelly A, Calamante F. Improved partial volume correction for single inversion time arterial spin labeling data. *Magn Reson Med* 2013; **69**: 531–537.

126 Chappell MA, Groves AR, MacIntosh BJ, Donahue MJ, Jezzard P, Woolrich MW. Partial volume correction of multiple inversion time arterial spin labeling MRI data. *Magn Reson Med* 2011; **65**: 1173–1183.

127 Nishimura DG, Macovski A, Pauly JM, Conolly SM. MR angiography by selective inversion recovery. *Magn Reson Med* 1987; **4**: 193–202.

128 Wang SJ, Nishimura DG, Macovski A. Multiple-readout selective inversion recovery angiography. *Magn Reson Med* 1991; **17**: 244–251.

129 Edelman RR, Siewert B, Adamis M, Gaa J, Laub G, Wielopolski P. Signal targeting with alternating radiofrequency (STAR) sequences: Application to MR angiography. *Magn Reson Med* 1994; **31**: 233–238.

130 Sallustio F, Kern R, Gunther M, Szabo K, Griebe M, Meairs S *et al.* Assessment of Intracranial Collateral Flow by Using Dynamic Arterial Spin Labeling MRA and Transcranial Color-Coded Duplex Ultrasound. *Stroke* 2008; **39**: 1894–1897.

131 Wu H, Block WF, Turski PA, Mistretta CA, Johnson KM. Noncontrast-enhanced three-dimensional (3D) intracranial MR angiography using pseudocontinuous arterial spin labeling and accelerated 3D radial acquisition. *Magn Reson Med* 2013; **69**: 708–715.

132 van Osch MJP, Hendrikse J, Golay X, Bakker CJG, van der Grond J. Non-invasive visualization of collateral blood flow patterns of the circle of Willis by dynamic MR angiography. *Med Image Anal* 2006; **10**: 59–70.

133 Nakamura M, Yoneyama M, Tabuchi T, Takemura A, Obara M, Tatsuno S *et al.* Vessel-selective, non-contrast enhanced, time-resolved MR angiography with vessel-selective arterial spin labeling technique (CINEMA-SELECT) in intracranial arteries. *Radiol Phys Technol* 2013; **6**: 327–334.

134 Lindner T, Jensen-Kondering U, van Osch MJP, Jansen O, Helle M. 3D time-resolved vessel-selective angiography based on pseudo-continuous arterial spin labeling. *Magn Reson Imaging* 2015; **33**: 840–846.

135 Okell TW, Chappell MA, Woolrich MW, Günther M, Feinberg DA, Jezzard P. Vessel-encoded dynamic magnetic resonance angiography using arterial spin labeling. *Magn Reson Med* 2010; **64**: 698–706.

136 Priest AN, Graves MJ, Lomas DJ. Non-contrast-enhanced vascular magnetic resonance imaging using flow-dependent preparation with subtraction. *Magn Reson Med* 2012; **67**: 628–637.

137 Priest AN, Taviani V, Graves MJ, Lomas DJ. Improved artery-vein separation with acceleration-dependent preparation for non-contrast-enhanced magnetic resonance angiography. *Magn Reson Med* 2014; **72**: 699–706.

138 Obara M, Togao O, Yoneyama M, Okuaki T, Shibukawa S, Honda H *et al.* Acceleration-selective arterial spin labeling for intracranial MR angiography with improved visualization of cortical arteries and suppression of cortical veins. *Magn Reson Med* 2016. doi:10.1002/mrm.26275.
139 Koktzoglou I, Gupta N, Edelman RR. Nonenhanced extracranial carotid MR angiography using arterial spin labeling: improved performance with pseudocontinuous tagging. *J Magn Reson Imaging* 2011; **34**: 384–394.
140 Koktzoglou I, Meyer JR, Ankenbrandt WJ, Giri S, Piccini D, Zenge MO *et al.* Nonenhanced arterial spin labeled carotid MR angiography using three-dimensional radial balanced steady-state free precession imaging. *J Magn Reson Imaging* 2015; **41**: 1150–1156.
141 MacIntosh BJ, Sideso E, Donahue MJ, Chappell MA, Günther M, Handa A *et al.* Intracranial hemodynamics is altered by carotid artery disease and after endarterectomy: a dynamic magnetic resonance angiography study. *Stroke* 2011; **42**: 979–984.
142 Günther M, Warmuth C, Zimmer C. Sub-millimeter Dynamic Spin Labeling Cerebral 2D-Angiography with 40ms Temporal Resolution. In: *Proceedings of the 10th Annual Meeting of ISMRM*. Honolulu, USA, 2002, p 1100.
143 Okell TW, Schmitt P, Bi X, Chappell MA, Tijssen RH, Miller KL *et al.* 4D Vessel-Encoded Arterial Spin Labeling Angiography. In: *Proceedings 19th Scientific Meeting, ISMRM*. Montreal, Canada, 2011, p 4034.
144 Kopeinigg D, Bammer R. Time-resolved angiography using inflow subtraction (TRAILS). *Magn Reson Med* 2014; **72**: 669–678.
145 Okell TW, Chappell MA, Schulz UG, Jezzard P. A kinetic model for vessel-encoded dynamic angiography with arterial spin labeling. *Magn Reson Med* 2012; **68**: 969–979.
146 Wu H, Block WF, Turski PA, Mistretta CA, Rusinak DJ, Wu Y *et al.* Noncontrast dynamic 3D intracranial MR angiography using pseudo-continuous arterial spin labeling (PCASL) and accelerated 3D radial acquisition. *J Magn Reson Imaging* 2014; **39**: 1320–1326.
147 Bi X, Weale P, Schmitt P, Zuehlsdorff S, Jerecic R. Non-contrast-enhanced four-dimensional (4D) intracranial MR angiography: A feasibility study. *Magn Reson Med* 2010; **63**: 835–841.
148 Yan L, Wang S, Zhuo Y, Wolf RL, Stiefel MF, An J *et al.* Unenhanced dynamic MR angiography: high spatial and temporal resolution by using true FISP-based spin tagging with alternating radiofrequency. *Radiology* 2010; **256**: 270–279.
149 Song HK, Yan L, Smith RX, Xue Y, Rapacchi S, Srinivasan S *et al.* Noncontrast enhanced four-dimensional dynamic MRA with golden angle radial acquisition and K-space weighted image contrast (KWIC) reconstruction. *Magn Reson Med* 2014; **72**: 1541–1551.
150 Yan L, Salamon N, Wang DJJ. Time-resolved noncontrast enhanced 4-D dynamic magnetic resonance angiography using multibolus TrueFISP-based spin tagging with alternating radiofrequency (TrueSTAR). *Magn Reson Med* 2014; **71**: 551–560.
151 Storey P, Li W, Chen Q, Edelman RR. Flow artifacts in steady-state free precession cine imaging. *Magn Reson Med* 2004; **51**: 115–122.
152 Koktzoglou I, Giri S, Piccini D, Grodzki DM, Flanagan O, Murphy IG *et al.* Arterial spin labeled carotid MR angiography: A phantom study examining the impact of technical and hemodynamic factors. *Magn Reson Med* 2016; **75**: 295–301.
153 Griswold MA, Jakob PM, Heidemann RM, Nittka M, Jellus V, Wang J *et al.*

Generalized Autocalibrating Partially Parallel Acquisitions (GRAPPA). *Magn Reson Med* 2002; **47**: 1202–1210.

154 Pruessmann KP, Weiger M, Scheidegger MB, Boesiger P. SENSE: Sensitivity encoding for fast MRI. *Magn Reson Med* 1999; **42**: 952–962.

155 Katoh M, Stuber M, Buecker A, Günther RW, Spuentrup E. Spin-labeling coronary MR angiography with steady-state free precession and radial k-space sampling: initial results in healthy volunteers. *Radiology* 2005; **236**: 1047–1052.

156 Okell TW, Chappell MA, Jezzard P. A theoretical framework for quantifying blood volume flow rate from dynamic angiographic data and application to vessel-encoded arterial spin labeling MRI. *Med Image Anal* 2013; **17**: 1025–1036.

157 Haller S, Zaharchuk G, Thomas DL, Lovblad K-O, Barkhof F, Golay X. Arterial spin labeling perfusion of the brain: emerging clinical applications. *Radiology* 2016; **281**:337-356.

158 Mirasol R V., Bokkers RPH, Hernandez DA, Merino JG, Luby M, Warach S *et al.* Assessing reperfusion with whole-brain arterial spin labeling a noninvasive alternative to gadolinium. *Stroke* 2014; **45**: 456–461.

159 Wang J, Aguirre GK, Kimberg DY, Roc AC, Li L, Detre JA. Arterial spin labeling perfusion fMRI with very low task frequency. *Magn Reson Med* 2003; **49**: 796–802.

160 Segerdahl AR, Mezue M, Okell TW, Farrar JT, Tracey I. The dorsal posterior insula subserves a fundamental role in human pain. *Nat Neurosci* 2015; **18**: 499–500.

161 Bulte DP, Kelly M, Germuska M, Xie J, Chappell MA, Okell TW *et al.* Quantitative measurement of cerebral physiology using respiratory-calibrated MRI. *Neuroimage* 2012; **60**: 582–591.

162 Gauthier CJ, Hoge RD. Magnetic resonance imaging of resting OEF and CMRO2 using a generalized calibration model for hypercapnia and hyperoxia. *Neuroimage* 2012; **60**: 1212–1225.

163 Brumm KP, Perthen JE, Liu TT, Haist F, Ayalon L, Love T. An arterial spin labeling investigation of cerebral blood flow deficits in chronic stroke survivors. *Neuroimage* 2010; **51**: 995–1005.

164 Harston GWJ, Okell TW, Sheerin F, Schulz U, Mathieson P, Reckless I *et al.* Quantification of Serial Cerebral Blood Flow in Acute Stroke Using Arterial Spin Labeling. *Stroke* 2017; **48**: 123–130.

165 de Havenon A, Haynor DR, Tirschwell DL, Majersik JJ, Smith G, Cohen W *et al.* Association of Collateral Blood Vessels Detected by Arterial Spin Labeling Magnetic Resonance Imaging With Neurological Outcome After Ischemic Stroke. *JAMA Neurol* 2017; **74**: 453–458.

166 Bokkers RPH, van Osch MJP, van der Worp HB, de Borst GJ, Mali WPTM, Hendrikse J. Symptomatic carotid artery stenosis: impairment of cerebral autoregulation measured at the brain tissue level with arterial spin-labeling MR imaging. *Radiology* 2010; **256**: 201–208.

167 Richter V, Helle M, van Osch MJP, Lindner T, Gersing AS, Tsantilas P *et al.* MR Imaging of Individual Perfusion Reorganization Using Superselective Pseudocontinuous Arterial Spin-Labeling in Patients with Complex Extracranial Steno-Occlusive Disease. *Am J Neuroradiol* 2017; **38**: 703–711.

168 Yu SL, Wang R, Wang R, Wang S, Yao YQ, Zhang D *et al.* Accuracy of vessel-encoded pseudocontinuous arterial spin-labeling in identification of feeding arteries in patients with intracranial arteriovenous malformations. *Am J Neuroradiol* 2014; **35**: 65–71.

169 Jensen-Kondering U, Lindner T, Van Osch MJP, Rohr A, Jansen O, Helle M.

Superselective pseudo-continuous arterial spin labeling angiography. *Eur J Radiol* 2015; **84**: 1758–1767.

170 Noguchi T, Kawashima M, Irie H, Ootsuka T, Nishihara M, Matsushima T *et al.* Arterial spin-labeling MR imaging in moyamoya disease compared with SPECT imaging. *Eur J Radiol* 2011; **80**: e557-62.

171 Ni WW, Christen T, Rosenberg J, Zun Z, Moseley ME, Zaharchuk G. Imaging of cerebrovascular reserve and oxygenation in Moyamoya disease. *J Cereb Blood Flow Metab* 2017; **37**: 1213–1222.

172 Alsop DC, Dai W, Grossman M, Detre JA. Arterial spin labeling blood flow MRI: Its Role in the early characterization of Alzheimer's disease. J. Alzheimer's Dis. 2010; **20**: 871–880.

173 Benedictus MR, Leeuwis AE, Binnewijzend MAA, Kuijer JPA, Scheltens P, Barkhof F *et al.* Lower cerebral blood flow is associated with faster cognitive decline in Alzheimer's disease. *Eur Radiol* 2017; **27**: 1169–1175.

174 Schuff N, Matsumoto S, Kmiecik J, Studholme C, Du A, Ezekiel F *et al.* Cerebral blood flow in ischemic vascular dementia and Alzheimer's disease, measured by arterial spin-labeling magnetic resonance imaging. *Alzheimer's Dement* 2009; **5**: 454–462.

175 Gao Y-Z, Zhang J-J, Liu H, Wu G-Y, Xiong L, Shu M. Regional Cerebral Blood Flow and Cerebrovascular Reactivity in Alzheimer's Disease and Vascular Dementia Assessed by Arterial Spin- labeling Magnetic Resonance Imaging. *Curr Neurovasc Res* 2013; **10**: 49–53.

176 Verfaillie SCJ, Adriaanse SM, Binnewijzend MAA, Benedictus MR, Ossenkoppele R, Wattjes MP *et al.* Cerebral perfusion and glucose metabolism in Alzheimer's disease and frontotemporal dementia: two sides of the same coin? *Eur Radiol* 2015; **25**: 3050–3059.

177 Ye J, Bhagat SK, Li H, Luo X, Wang B, Liu L *et al.* Differentiation between recurrent gliomas and radiation necrosis using arterial spin labeling perfusion imaging. *Exp Ther Med* 2016; **11**: 2432–2436.

178 Kong L, Chen H, Yang Y, Chen L. A meta-analysis of arterial spin labelling perfusion values for the prediction of glioma grade. *Clin Radiol* 2017; **72**: 255–261.

179 Wang P, Li J, Diao Q, Lin YK, Zhang J, Li L *et al.* Assessment of glioma response to radiotherapy using 3D pulsed-continuous arterial spin labeling and 3D segmented volume. *Eur J Radiol* 2016; **85**: 1987–1992.

180 Lu Y, Luan S, Liu L, Xiong J, Wen J, Qu J *et al.* Evaluation of the applicability of territorial arterial spin labeling in meningiomas for presurgical assessments compared with 3-dimensional time-of-flight magnetic resonance angiography. *Eur Radiol* 2017; **In press**: DOI: 10.1007/s00330-017-4760-9.

181 Guo X, Xu S, Wang G, Zhang Y, Guo L, Zhao B. Asymmetry of cerebral blood flow measured with three-dimensional pseudocontinuous arterial spin-labeling mr imaging in temporal lobe epilepsy with and without mesial temporal sclerosis. *J Magn Reson Imaging* 2015; **42**: 1386–1397.

182 Kim BS, Lee ST, Yun TJ, Lee SK, Paeng JC, Jun J *et al.* Capability of arterial spin labeling MR imaging in localizing seizure focus in clinical seizure activity. *Eur J Radiol* 2016; **85**: 1295–1303.

183 Amann M, Achtnichts L, Hirsch JG, Naegelin Y, Gregori J, Weier K *et al.* 3D GRASE arterial spin labelling reveals an inverse correlation of cortical perfusion with the white matter lesion volume in MS. *Mult Scler J* 2012; **18**: 1570–1576.

184 Paling D, Thade Petersen E, Tozer DJ, Altmann DR, Wheeler-Kingshott CA, Kapoor

R *et al.* Cerebral Arterial Bolus Arrival Time is Prolonged in Multiple Sclerosis and Associated with Disability. *J Cereb Blood Flow Metab* 2014; **34**: 34–42.

185 Koudriavtseva T, Plantone D, Renna R, Inglese M. Brain perfusion by arterial spin labeling MRI in multiple sclerosis. *J Neurol* 2015; **262**: 1769–1771.

186 Barlow KM, Marcil LD, Dewey D, Carlson HL, MacMaster FP, Brooks BL *et al.* Cerebral Perfusion Changes in Post-Concussion Syndrome: A Prospective Controlled Cohort Study. *J Neurotrauma* 2017; **34**: 996–1004.

187 Duhameau B, Ferré J-C, Jannin P, Gauvrit J-Y, Vérin M, Millet B *et al.* Chronic and treatment-resistant depression: A study using arterial spin labeling perfusion MRI at 3Tesla. *Psychiatry Res Neuroimaging* 2010; **182**: 111–116.

188 Scheef L, Manka C, Daamen M, Kühn K-U, Maier W, Schild HH *et al.* Resting-state perfusion in nonmedicated schizophrenic patients: a continuous arterial spin-labeling 3.0-T MR study. *Radiology* 2010; **256**: 253–60.

189 Schuff N, Zhang Y, Zhan W, Lenoci M, Ching C, Boreta L *et al.* Patterns of altered cortical perfusion and diminished subcortical integrity in posttraumatic stress disorder: An MRI study. *Neuroimage* 2011; **54**: S62–S68.

190 Okell TW. *Assessment of collateral blood flow in the brain using magnetic resonance imaging*. PhD Thesis, University of Oxford, UK. 2011.https://ora.ox.ac.uk/objects/uuid:7e63bcf2-22bf-49e5-81ec-1644217605ae.

Figure Captions

Figure 1: Part a) shows the pulse sequence preparation elements for pseudo-continuous ASL (pCASL), consisting of a train of selective RF pulses (of low flip angle α and zero phase) in combination with suitable gradients in the direction of flow. The pulse train used as the control, which has pulses with the same flip angle but alternating phase, and which is substituted for the labeling RF pulse train, is also shown. Part b) shows the repeating modulation of M_z as a function of the phase accumulated between RF pulses that is imposed on the flowing spins by the gradient shown in (a). Since the rate of accumulation of phase is proportional to the distance of the spins from the labeling plane, the *x*-axis is equivalent to distance. Note that since selective RF pulses are used the flowing spins only experience the transition region shown in red, which causes their magnetization vectors to invert as they pass through the labeling plane (i.e., left to right in the figure). The dashed lines show the parts of the modulation pattern (locations) for which the spins are outside the influence of the selective RF pulses used.

Figure 2: Schematic of some of the principal flavours of ASL pulse sequence. In each case the green box shows the region of the label and the blue box shows the region of the control pulse. a) shows a 'conventional' CASL pulse sequence and its accompanying label/control locations. b) shows a PICORE PASL pulse sequence, in which the control pulse is an off-resonance pulse (not actually location specific). c) shows a FAIR pulse sequence and labeling figure, in which the label is created with a non-slice-selective inversion pulse, and the control is a slice-selective inversion. Finally, d) shows the QUIPSS-II PASL sequence, in which a saturation (red box) is added at time TI_1 to the labeling region to better control the temporal duration of the bolus of labeled blood.

Figure 3: Multi-delay ASL strategies: in order to sample the dynamics of labeled blood flowing into the tissue to allow for arrival time estimation and kinetic model fitting, multiple label and control images can be acquired with different post-labeling delays (top). Alternatively, a Look-Locker strategy can be employed consisting of multiple low-flip angle readouts following each label or control preparation to sample the blood signal at different times after labeling (middle). In time-encoded CASL or PCASL the labeling period is split up into a series of blocks. If these blocks are alternated between label and control states in different ways across different imaging cycles according to a Hadamard encoding matrix, then the perfusion signal arising from each of these separate labeling blocks can be "decoded" in post-processing, yielding multiple images with different effective post-labeling delays (bottom). [Figure originally published in "Introduction to Perfusion Quantification using Arterial Spin Labeling" by Michael Chappell, Bradley MacIntosh and Thomas Okell, Oxford University Press, and reproduced with permission].

Figure 4: Schematic of vessel-selective ASL for labeling the four main brain-feeding arteries: vessel-selectivity can be achieved by targeting individual arteries of interest, using a labeling slab or spot, before moving on to the next artery to build up individual maps of the vascular territories by simple subtraction of label and control images (top). Alternatively, different combinations of vessels can be labeled or controlled across multiple imaging cycles, uniquely encoding the signal from each artery that can then be decoded in post-processing (bottom). Although more complex to process, the vessel-

encoded approach results in perfusion signal from all arteries across all cycles, boosting SNR when the images are combined.

Figure 5: Example time series plots from the 'standard' model for ASL kinetics comparing PASL and pCASL. Unless otherwise specified arterial transit time (Δt) = 0.7 seconds (PASL) or 0.9 seconds (pCASL), T_1=1.65 seconds, bolus duration = 0.8 seconds (PASL), 1.8 seconds (pCASL) following Alsop et al.[29] The plots show arterial input functions with varying arterial transit time (a,b), residue function for varying T_1 (c), voxel magnetization for varying arterial transit time (d,e) and varying T_1 (f,g).

Figure 6: Partial volume effects in ASL and methods for correction illustrated in simulated data created using PV estimates from structural data in an individual and different spatial distributions (a-c) of GM CBF ('True'). 'Standard' refers to the estimated CBF map using standard quantifications, Spatial PV refers to the spatial method of Chappell et al.[126] and LR corresponds to the linear regression method of Asllani et al.[124] with different kernel sizes. Figure reproduced with permission from Chappell et al.[126] (Figure 2).

Figure 7: Example transverse maximum intensity projection from a 4D vessel-encoded ASL angiogram with bSSFP readout.[92] Color represents the arterial origin of the blood signal: right/left internal carotid artery (red/green), right/left vertebral artery (blue/magenta).

Figure 8: Schematic of strategies for dynamic ASL angiography: For PASL (top row) labeling (orange block) occurs quickly, so the addition of a time-resolved readout, in which the same set of k-space lines are repeatedly acquired (green blocks), allows the generation of images showing the inflow of labeled blood. Since only a subset of k-space lines can typically be acquired per ASL preparation this process is repeated until all lines of k-space have been acquired for both label and control conditions. For CASL or PCASL, one method to obtain temporal resolution is to acquire a single image after labeling the blood, but to vary the label duration (middle row), which in turn varies the distance into the vascular tree that the labeled blood has travelled. Alternatively, a single long label duration can be used followed by a time-resolved readout. In this case the first image shows the vascular tree filled with labeled blood and subsequent images show washout of the bolus. However, "inflow subtraction", in which each subsequent image is subtracted from the first, results in images showing inflow rather than outflow for a more intuitive visualization. Images are shown in inverted contrast and control cycles are omitted for clarity.

Figure 9: Preliminary data showing vessel-encoded pCASL perfusion imaging (top left) and angiography (bottom) in a patient with a history of transient ischaemic attack, alongside time-of-flight angiography data (top right) for comparison. Color represents the arterial origin of the blood signal as per Figure 7, with one example perfusion slice shown separately for each artery in grayscale for clarity. Reduced blood flow is apparent in the left vertebral artery (LVA, orange arrows). Significant collateral flow from the right internal carotid artery (RICA) through the posterior communicating artery to the right posterior cerebral artery is also observed (yellow arrows), and to a lesser extent on the left side (white arrows), perhaps to help compensate for the limited

blood supply arising from the LVA. Adapted from Okell.[190] Data were acquired in collaboration with Dr Ursula Schulz.

Figure 10: Vessel-encoded pCASL dynamic angiography (top) and a time-of-flight (TOF) angiography maximum intensity projection (MIP, bottom) in a patient with arteriovenous malformation (AVM). Color represents the arterial origin of the blood signal as per Figure 7. Selected frames are shown demonstrating the major feeding vessels to the AVM from both the RICA via lateral (purple arrows) and medial (yellow arrows) branches of the right middle cerebral artery, and the LICA via the anterior cerebral arteries (orange arrows). The times shown are relative to the start of the VEPCASL labeling. Similar features can be observed in the TOF MIP, although some vessels are obscured due to overlying static tissue that is subtracted away in the VEPCASL data. Further work is required to separate the blood signals arising from smaller arterial branches, as has been demonstrated with super-selective ASL techniques,[169] and to better visualize venous drainage. Adapted from Okell.[190] Data were acquired in collaboration with Dr Natalie Voets.

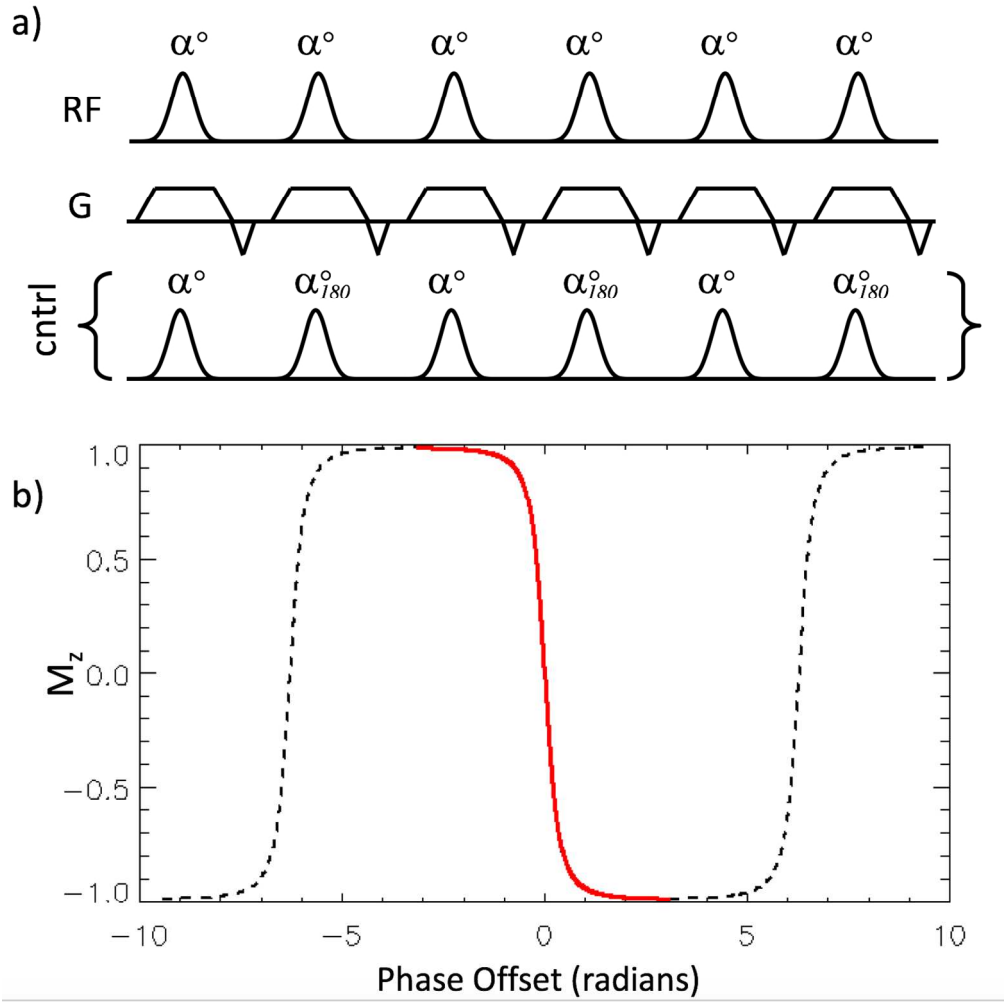

Figure 1: Part a) shows the pulse sequence preparation elements for pseudo-continuous ASL (pCASL), consisting of a train of selective RF pulses (of low flip angle and zero phase) in combination with suitable gradients in the direction of flow. The pulse train used as the control, which has pulses with the same flip angle but alternating phase, and which is substituted for the labeling RF pulse train, is also shown. Part b) shows the repeating modulation of Mz as a function of the phase accumulated between RF pulses that is imposed on the flowing spins by the gradient shown in (a). Since the rate of accumulation of phase is proportional to the distance of the spins from the labeling plane, the x-axis is equivalent to distance. Note that since selective RF pulses are used the flowing spins only experience the transition region shown in red, which causes their magnetization vectors to invert as they pass through the labeling plane (i.e., left to right in the figure). The dashed lines show the parts of the modulation pattern (locations) for which the spins are outside the influence of the selective RF pulses used.

263x264mm (144 x 144 DPI)

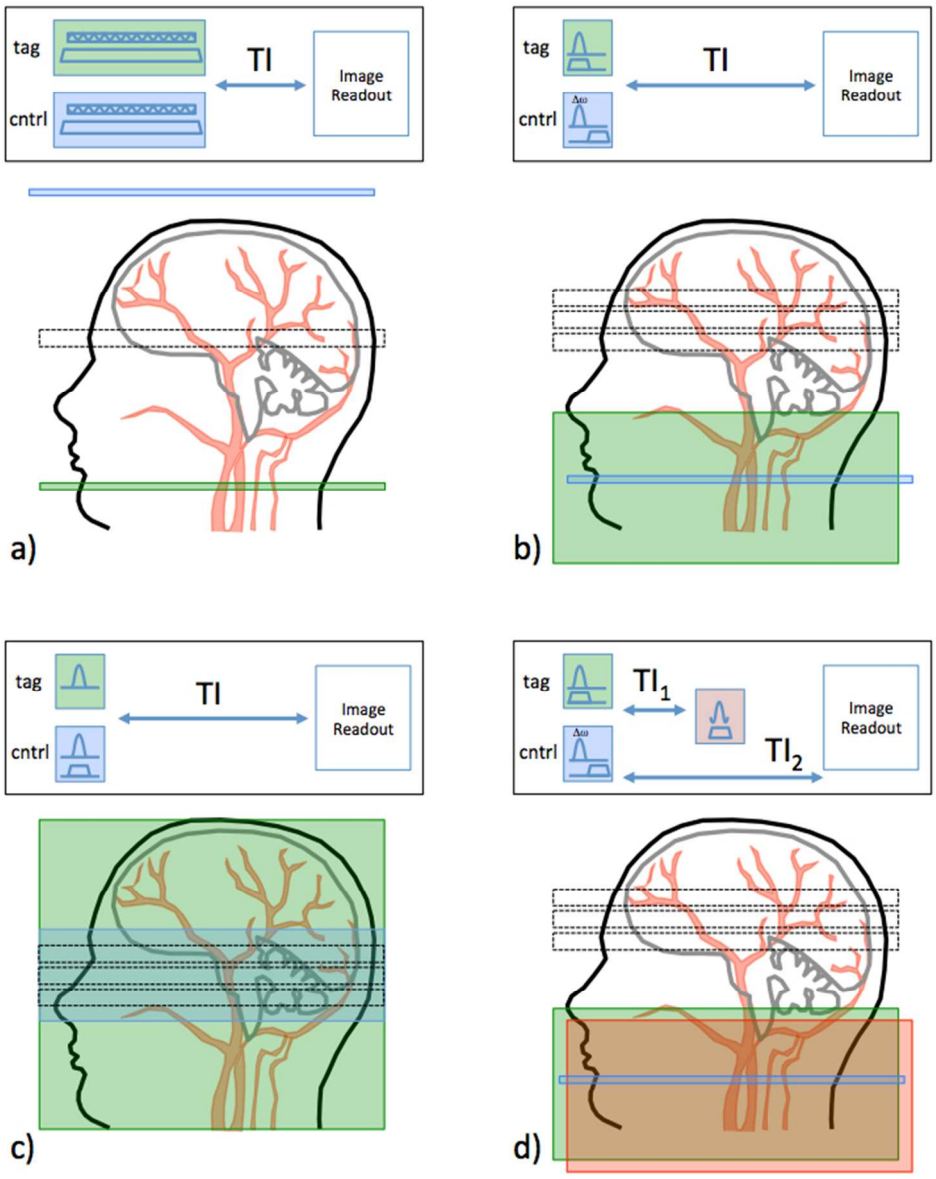

Figure 2: Schematic of some of the principal flavours of ASL pulse sequence. In each case the green box shows the region of the label and the blue box shows the region of the control pulse. a) shows a 'conventional' CASL pulse sequence and its accompanying label/control locations. b) shows a PICORE PASL pulse sequence, in which the control pulse is an off-resonance pulse (not actually location specific). c) shows a FAIR pulse sequence and labeling figure, in which the label is created with a non-slice-selective inversion pulse, and the control is a slice-selective inversion. Finally, d) shows the QUIPSS-II PASL sequence, in which a saturation (red box) is added at time TI1 to the labeling region to better control the temporal duration of the bolus of labeled blood.

269x322mm (72 x 72 DPI)

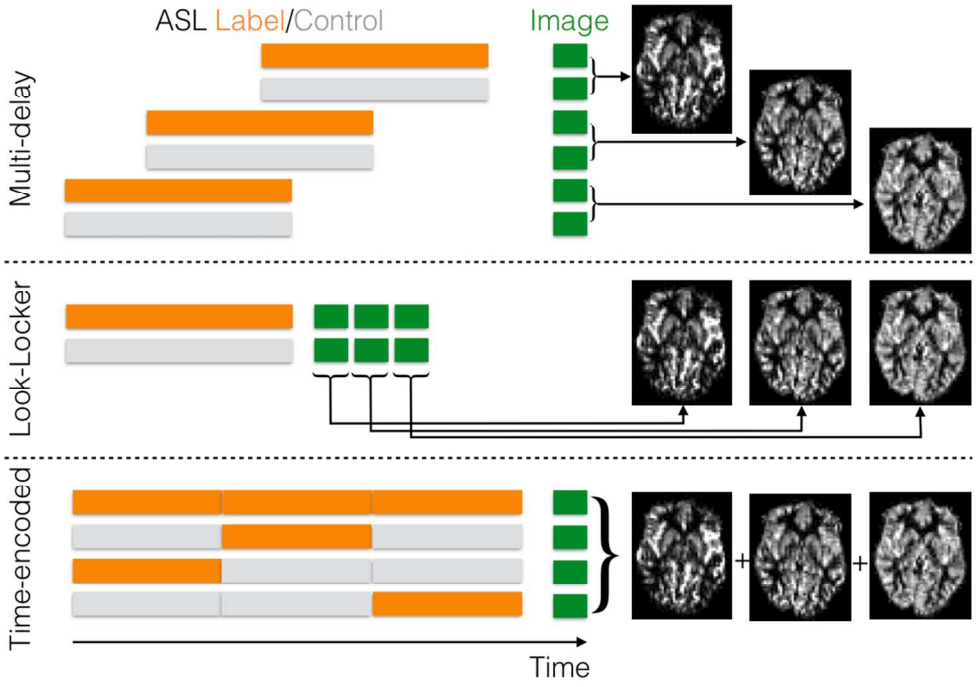

Figure 3: Multi-delay ASL strategies: in order to sample the dynamics of labeled blood flowing into the tissue to allow for arrival time estimation and kinetic model fitting, multiple label and control images can be acquired with different post-labeling delays (top). Alternatively, a Look-Locker strategy can be employed consisting of multiple low-flip angle readouts following each label or control preparation to sample the blood signal at different times after labeling (middle). In time-encoded CASL or PCASL the labeling period is split up into a series of blocks. If these blocks are alternated between label and control states in different ways across different imaging cycles according to a Hadamard encoding matrix, then the perfusion signal arising from each of these separate labeling blocks can be "decoded" in post-processing, yielding multiple images with different effective post-labeling delays (bottom). [Figure originally published in "Introduction to Perfusion Quantification using Arterial Spin Labeling" by Michael Chappell, Bradley MacIntosh and Thomas Okell, Oxford University Press, and reproduced with permission].

408x279mm (72 x 72 DPI)

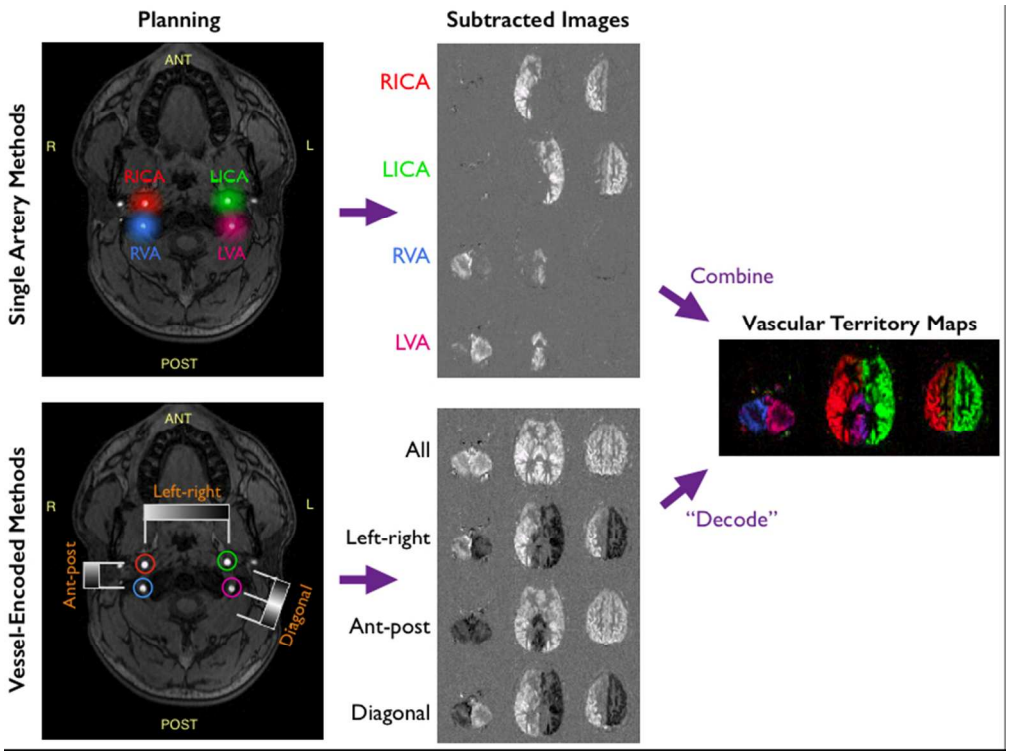

Figure 4: Schematic of vessel-selective ASL for labeling the four main brain-feeding arteries: vessel-selectivity can be achieved by targeting individual arteries of interest, using a labeling slab or spot, before moving on to the next artery to build up individual maps of the vascular territories by simple subtraction of label and control images (top). Alternatively, different combinations of vessels can be labeled or controlled across multiple imaging cycles, uniquely encoding the signal from each artery that can then be decoded in post-processing (bottom). Although more complex to process, the vessel-encoded approach results in perfusion signal from all arteries across all cycles, boosting SNR when the images are combined.

146x108mm (150 x 150 DPI)

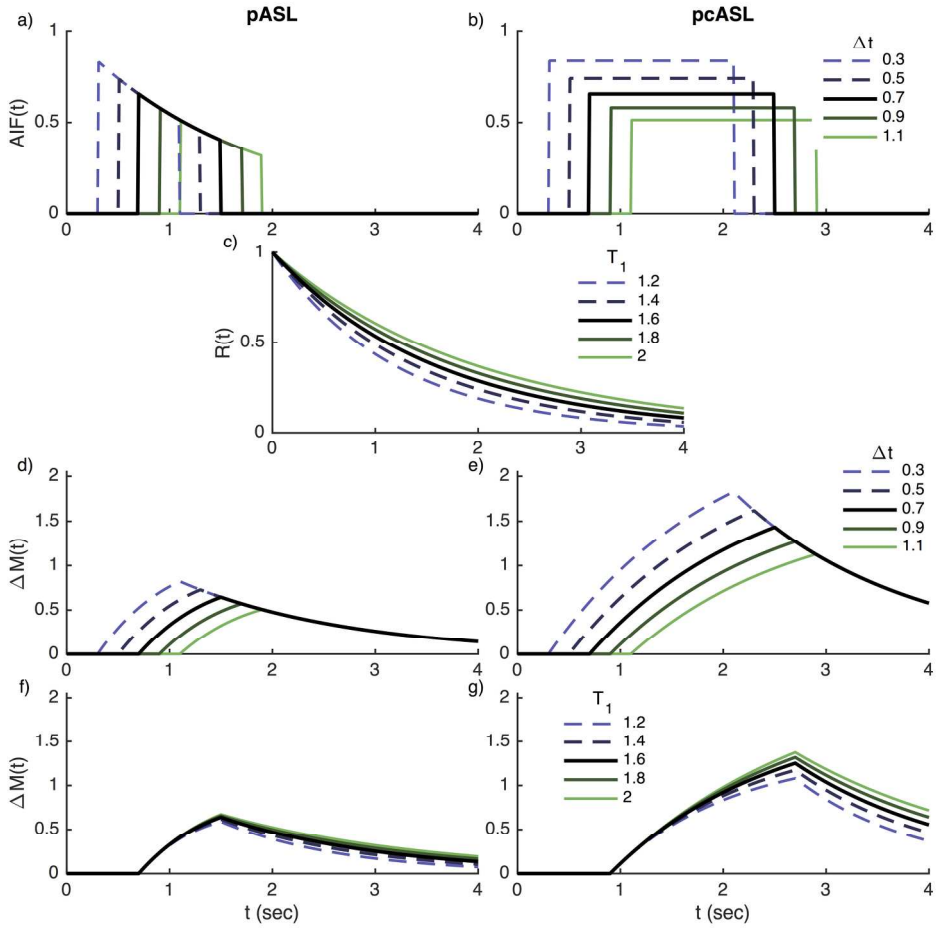

Figure 5: Example time series plots from the 'standard' model for ASL kinetics comparing PASL and pCASL. Unless otherwise specified arterial transit time (Δt) = 0.7 seconds (PASL) or 0.9 seconds (pCASL), T1=1.65 seconds, bolus duration = 0.8 seconds (PASL), 1.8 seconds (pCASL) following Alsop et al.29 The plots show arterial input functions with varying arterial transit time (a,b), residue function for varying T1 (c), voxel magnetization for varying arterial transit time (d,e) and varying T1 (f,g).

193x189mm (300 x 300 DPI)

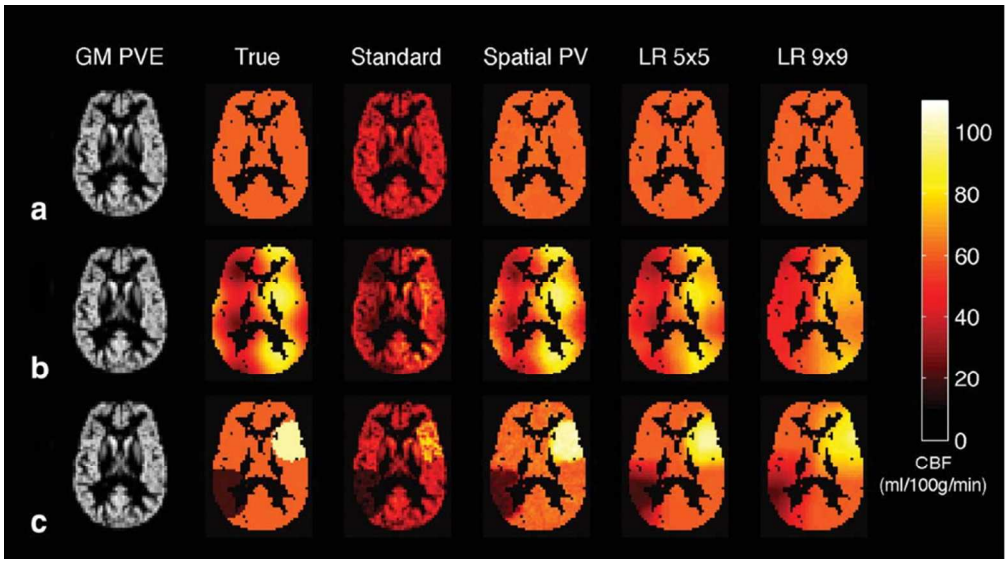

Figure 6: Partial volume effects in ASL and methods for correction illustrated in simulated data created using PV estimates from structural data in an individual and different spatial distributions (a-c) of GM CBF ('True'). 'Standard' refers to the estimated CBF map using standard quantifications, Spatial PV refers to the spatial method of Chappell et al.112 and LR corresponds to the linear regression method of Asllani et al.110 with different kernel sizes. Figure reproduced with permission from Chappell et al.112 (Figure 2).

366x202mm (72 x 72 DPI)

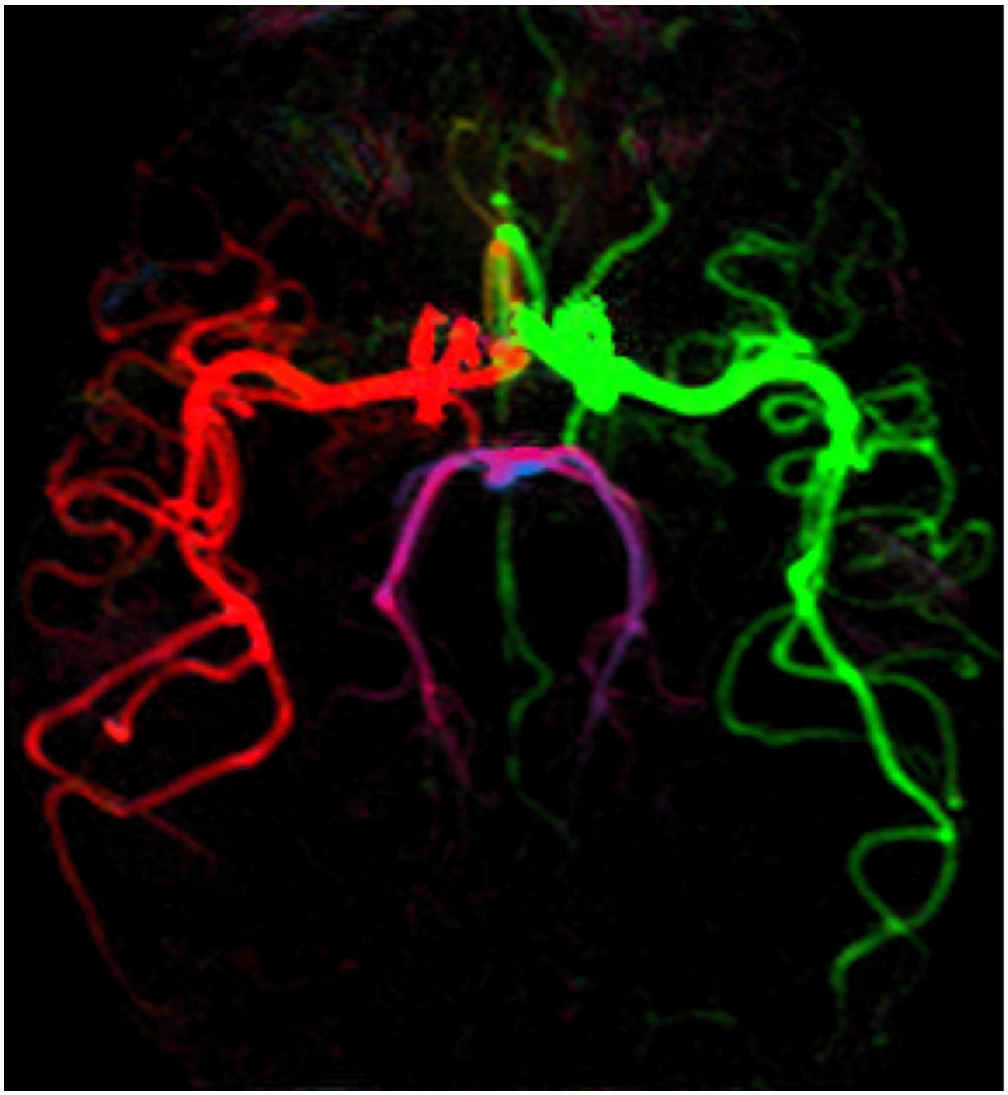

Figure 7: Example transverse maximum intensity projection from a 4D vessel-encoded ASL angiogram with bSSFP readout.73 Color represents the arterial origin of the blood signal: right/left internal carotid artery (red/green), right/left vertebral artery (blue/magenta).

254x275mm (72 x 72 DPI)

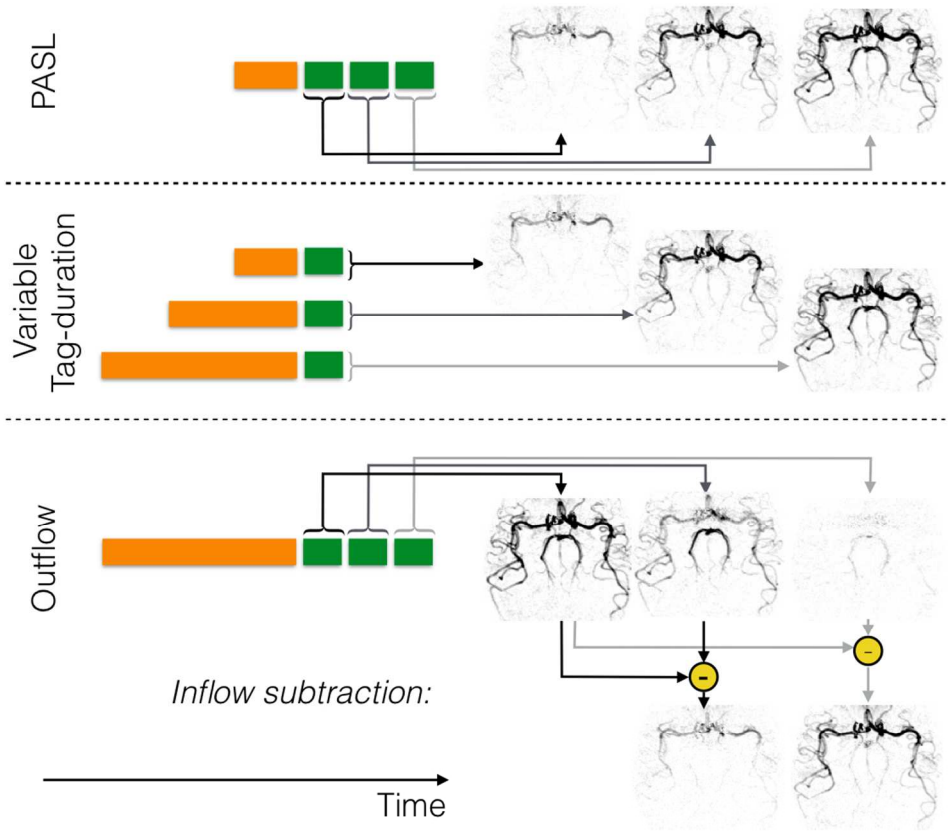

Figure 8: Schematic of strategies for dynamic ASL angiography: For PASL (top row) labeling (orange block) occurs quickly, so the addition of a time-resolved readout, in which the same set of k-space lines are repeatedly acquired (green blocks), allows the generation of images showing the inflow of labeled blood. Since only a subset of k-space lines can typically be acquired per ASL preparation this process is repeated until all lines of k-space have been acquired for both label and control conditions. For CASL or PCASL, one method to obtain temporal resolution is to acquire a single image after labeling the blood, but to vary the label duration (middle row), which in turn varies the distance into the vascular tree that the labeled blood has travelled. Alternatively, a single long label duration can be used followed by a time-resolved readout. In this case the first image shows the vascular tree filled with labeled blood and subsequent images show washout of the bolus. However, "inflow subtraction", in which each subsequent image is subtracted from the first, results in images showing inflow rather than outflow for a more intuitive visualization. Images are shown in inverted contrast and control cycles are omitted for clarity.

416x346mm (72 x 72 DPI)

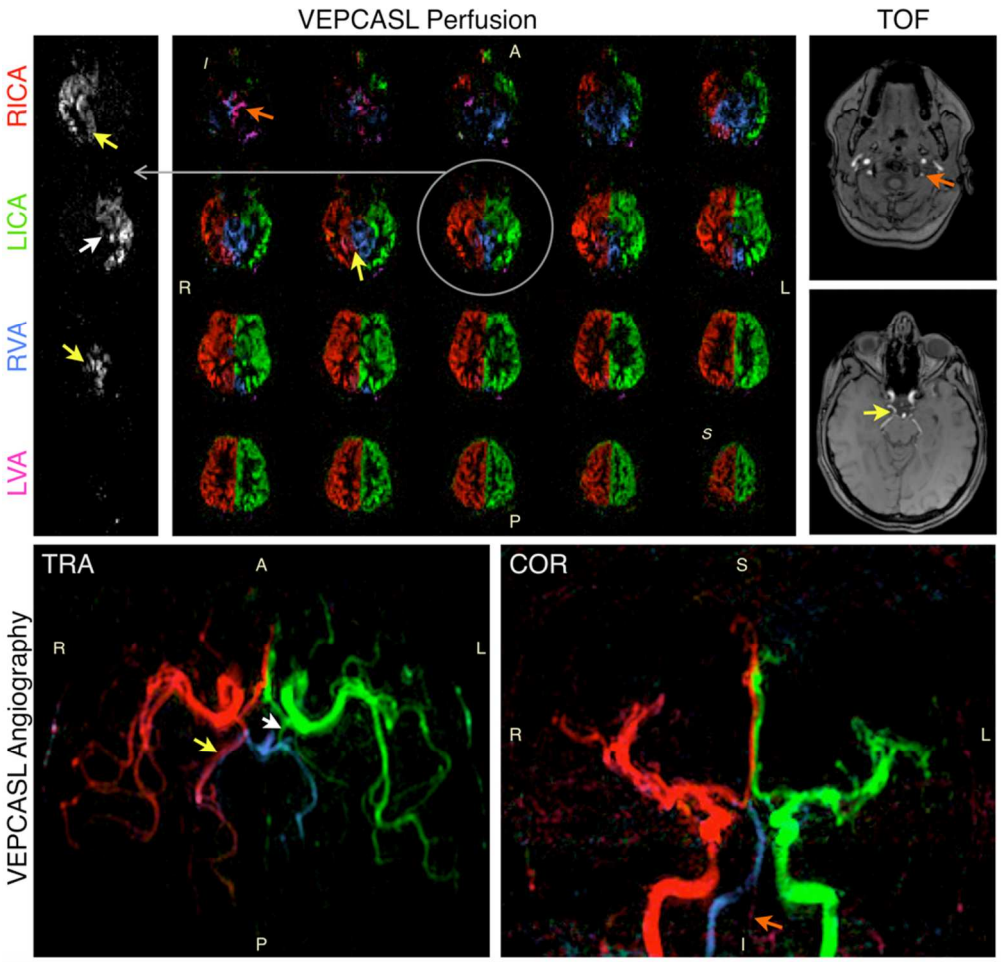

Figure 9: Preliminary data showing vessel-encoded pCASL perfusion imaging (top left) and angiography (bottom) in a patient with a history of transient ischaemic attack, alongside time-of-flight angiography data (top right) for comparison. Color represents the arterial origin of the blood signal as per Figure 7, with one example perfusion slice shown separately for each artery in grayscale for clarity. Reduced blood flow is apparent in the left vertebral artery (LVA, orange arrows). Significant collateral flow from the right internal carotid artery (RICA) through the posterior communicating artery to the right posterior cerebral artery is also observed (yellow arrows), and to a lesser extent on the left side (white arrows), perhaps to help compensate for the limited blood supply arising from the LVA. Adapted from Okell.175 Data were acquired in collaboration with Dr Ursula Schulz.

361x346mm (72 x 72 DPI)

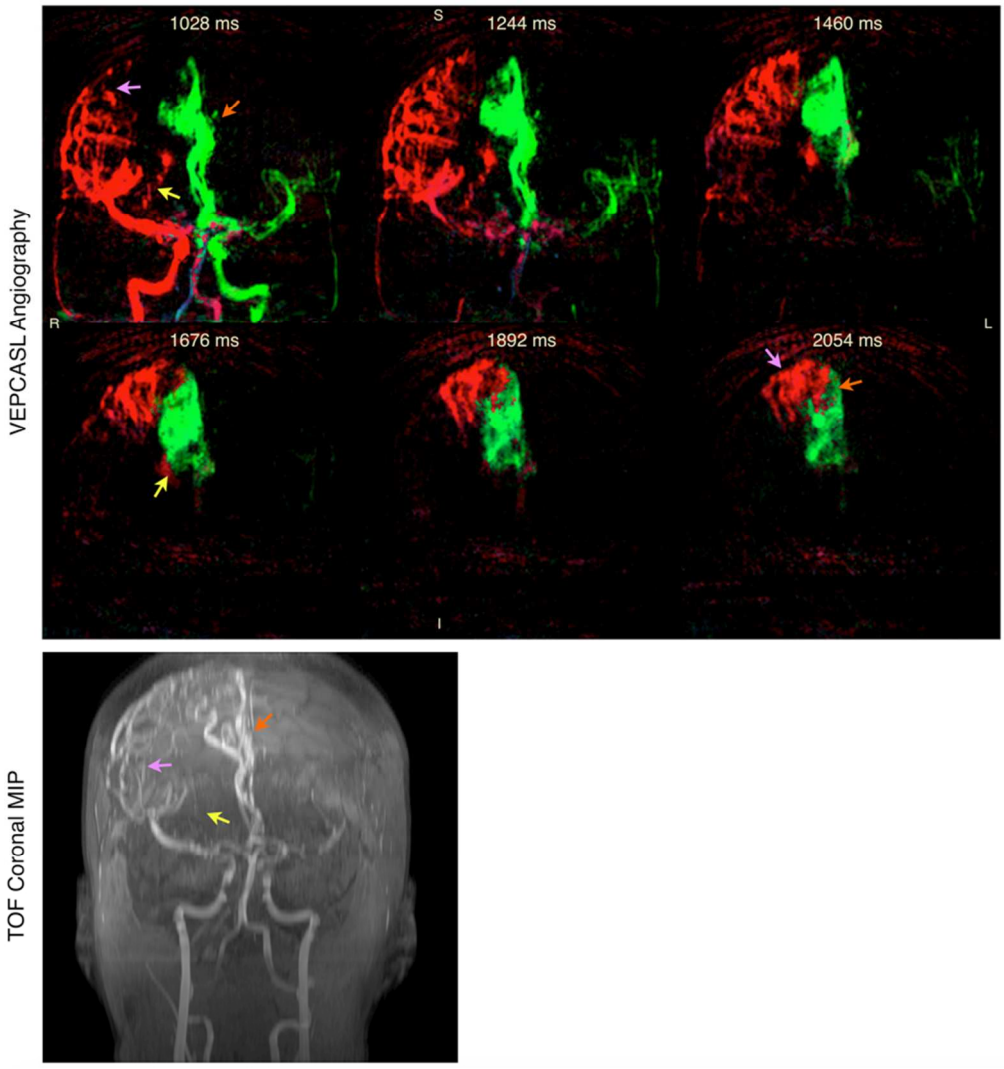

Figure 10: Vessel-encoded pCASL dynamic angiography (top) and a time-of-flight (TOF) angiography maximum intensity projection (MIP, bottom) in a patient with arteriovenous malformation (AVM). Color represents the arterial origin of the blood signal as per Figure 7. Selected frames are shown demonstrating the major feeding vessels to the AVM from both the RICA via lateral (purple arrows) and medial (yellow arrows) branches of the right middle cerebral artery, and the LICA via the anterior cerebral arteries (orange arrows). The times shown are relative to the start of the VEPCASL labeling. Similar features can be observed in the TOF MIP, although some vessels are obscured due to overlying static tissue that is subtracted away in the VEPCASL data. Further work is required to separate the blood signals arising from smaller arterial branches, as has been demonstrated with super-selective ASL techniques,154 and to better visualize venous drainage. Adapted from Okell.175 Data were acquired in collaboration with Dr Natalie Voets.

324x346mm (72 x 72 DPI)